

Final Report

PSI-6663

Date of Report: *31 August 2018*

Contract Number: *DTPH5615T00015*

Prepared for: *U.S. Department of Transportation – Pipeline and Hazardous Materials Safety Administration*

Project Title: *Natural Gas Pipeline Leak Rate Measurement System*

Prepared by: *Shin-Juh Chen and Michael B. Frish, Physical Sciences Inc.*

Contact Information: *Michael B. Frish, frish@psicorp.com, 978-738-8252*

For performance period covering: *01 October 2015 and 31 March 2018*

Project Summary:

Current natural gas leak survey tools find pipeline leaks by measuring the local methane concentration (in ppm) or the concentration integrated over line-of-sight path (in ppm-m), and lack the ability to measure the *leak rate* from a stand-off configuration. Direct leak rate measurement facilitates prioritizing repairs: In current practice, leaks exhibiting high gas concentrations are given repair priority. However, the concentration depends on wind; a small leak can lead to a locally high gas concentration when there is little wind to disperse the gas, and vice versa. Basing repair priority on leak rate rather than local concentration would; a) enhance public safety by identifying leaks that are continually emitting gas volumes that are potential explosion hazards as well as environmentally harmful; and b) reduce overall leakage, thus providing the economic benefits of reducing the cost of lost gas as well as the cost of low-priority repair.

Physical Sciences Inc. and Heath Consultants Inc. proposed an R&D project to fill this technology gap and advance the ability to detect low level leaks and provide a direct measure of the leak rate. This research project integrated advanced laser-based methane detection methods with novel deployment configurations and wind measurements to provide leak rate data in seconds during routine mobile leak surveys.

The major deployment configurations comprised side scanning RMLD systems that were handheld or fixed, spinning RMLD using a conical or cylindrical-scan of the laser light, extractive gas analyzer, two-dimensional gas leak rate imager (*a first of its kind*), and a suite of commercial sensors. A total of five major test campaigns, encompassing hundreds of tests and spanning over two years, were conducted using controlled and real-world leak scenarios; allowing the computation of fluxes from different configurations to be tested and validated.

The overall objective of developing mobile survey technologies and methodologies to locate and quantify flux of natural gas leaks was met. All research tasks were completed and all the deliverables were furnished. This project has generated much interest from the gas survey industries and resulted in additional and complementary tests. This project successfully demonstrated the leak rate measurement techniques and tools in real-world scenarios with some needing improvements for becoming a commercial product, namely the two-dimensional leak rate imager (RMLD-QGI). Moreover, the desire to measure both ethane and methane during leak surveys to differentiate natural gas leaks from other

methane sources (e.g. biogas) was identified as a preferred method of reducing false detections and their associated costs during mobile surveys. Ethane comprises about 10% of the natural gas composition, but is not present in biogas. Many of the developed technologies and lessons learned from this project are already implemented by project participant Heath Consultants Inc. into its commercial leak survey tools, and helping in the improvement of existing methodologies and development of future leak rate sensors.

Major Conclusions:

1. This PHMSA R&D project met the overall objective of developing mobile survey technologies and methodologies to locate and quantify flux of natural gas leaks. The research tasks were completed and all deliverables were met.
2. Using a combination of new and mature technologies, this project has successfully demonstrated the measurement of leak rates that is very important in the classification and prioritization for repairs. Moreover, these technologies enhanced routine mobile leak surveys and provided a rapid and cost-effective direct measure of the leak rate.
3. Using a proven commercial leak detection platform (RMLDTM), several configurations of this device provided methods for locating, identifying, and measuring the leak rates of methane in urban environments. These configurations, along with an onboard gas analyzer and leak rate imager, afforded critical demonstrations in real-world leak scenarios.
4. Spinning RMLD with cylindrical scans, compared to conical scans, was less sensitive to variation in wind (speed and direction) and height (sensor to ground) and simplifies data analyses. Faster scans were better than slower ones to accommodate variability in wind. Upwind sources measure low (or zero) flux despite high local concentrations; a critical attribute of the spinner technique.
5. The spinning RMLD is able to detect and quantify leaks smaller than 2 scfh in a 3m/s wind in less than 10 seconds with flux accuracy $\sim\pm 20\%$.
6. Extractive analyzers (point sensors) onboard mobile platforms required exceptionally high-sensitivity to detect small-sized methane leaks in urban environment in most scenarios due to its long time response limited by the refresh rate of the cell's internal volume and vehicle's speed in typical urban surveys.
7. Fixed open-path leak detector's fast response compared to the extractive analyzer is capable of detecting small leaks while installed on a survey vehicle moving at typical posted residential speed limit of 25mph.
8. The use of two fixed-position RMLDs on opposite sides of mobile survey vehicle enhanced the probability of detecting leaks having plume shapes dispersed by wind. Results indicated on several occasions that one or the other RMLD detected leaks that were not simultaneously seen by both.
9. Discussions within the Interstate Technology Regulatory Council (ITRC) recognized that emerging technologies which distinguish natural gas from other methane sources (e.g. biogas emitted by swamps, sewers, landfills, etc.) are desirable for mobile surveys, particularly for discriminating against false detection of gas leaks. The concurrent measurement of both methane and ethane is an option, ethane being a component of natural gas but not biogas. An ethane/methane gas analyzer is currently part of a leak survey vehicle (MobileGuardTM) operated by Heath Consultants Inc.

It is recommended that a backscatter TDLAS sensor that detects both ethane and methane be developed using the robust RMLD platform to confirm the source of methane with enhanced detection speed while covering a wide probed region during mobile surveys. No such open-path ethane/methane sensor is currently available.

10. A laser-based quantitative two-dimensional imaging methane leak detection system (RMLD-QGI) was able to identify leaks and quantify flow rates as small as 1 SCFH. This prototype has generated much interest from the gas survey industry and plans are in place to move this technology platform to a commercial product within the next few years.

Summary of Accomplishments:

1. This DOT-funded research with cost-share from Heath Consultants Inc. has generated much interest from the gas survey industries and led to additional and complementary field tests funded by NYSEARCH, SoCal, PG&E, Heath and PSI.
2. Using the conical-scan spinning RMLD mounted on the FluxMobile vehicle, 72 data files were collected for various conditions at the PSE&G test site located in Edison, NJ.
3. Using the cylindrical-scan spinning RMLD, 173 data files were collected for various conditions and spanned 83 distinct tests at the SoCal site in Commerce, CA.
4. Using the conical-scan spinning RMLD with remotely adjustable aim and mounted on the Flux Mobile vehicle, 15 leak sites were investigated in Westchester County, NY, near the ConEd facility in Elmsford, NY.
5. A suite of sensors including an extractive analyzer, fixed and handheld open-path sensors, a variety of other commercial sensors, and a wind sensor were utilized on two survey vehicles. The vehicles operated over a period of 11 months. More than 400 leak survey trips were completed in the areas surrounding Las Vegas, NV.
6. The field prototype imaging leak system was successfully assembled and tested in real-world leak scenarios. Over 51 field tests were conducted and analyzed over a period of 4 days in municipal settings near the SoCal facility in Pico Rivera, CA.
7. Software and graphical user interface were developed and improved over the course of this project to support system control, data acquisition, processing, analysis, recording, GPS positioning, and reporting functions to facilitate leak surveys in urban environments.
8. Both extractive analyzers and open-path leak detectors performed well during several months of operation in urban environment without incidence of any major mechanical failure in either extractive or open-path instruments.

Project Deliverables:

The following 10 items were completed and delivered:

1. Engaged with Team Members and Technical Advisors.
2. Conducted kick-off Team meeting that reviewed sensor system requirements, as well as the test and demonstration plan.
3. Developed multi-sensor system hardware and vehicle platform.
4. Developed data acquisition and data processing algorithms.
5. Integrated system hardware and software.
6. Conducted initial system development testing.
7. Conducted initial system field demonstration testing.
8. Conducted final quantitative system testing.
9. Prepared and submitted Quarterly status and progress reports and a final project report.
10. Attended and presented at conferences.

Table of Contents

Summary	1
Major Conclusions	3
Summary of Accomplishments	4
Project Deliverables	5
1. Motivation	10
2. Background	10
3. Project Objectives	12
4. Project Tasks	13
5. Task 1: Assembly of a Technical Advisory Committee (TAC)	13
6. Task 2: Team Meetings	14
7. Task 3: System Hardware Enhancements	14
8. Task 4: System Data Processing and Algorithms Development	19
9. Task 5: System Integration	24
10. Task 6: System Demonstration and Testing	28
11. Task 7: Peer Review	48
12. Task 8: Quarterly Progress Reports	48
13. Task 9: Final Report	48
14. Conferences and Publications	48
15. Summary and Conclusions	49
16. Acknowledgment	50

List of Figures

Figure 1.	Mobile leak detection using combination of highly sensitive point sensors and scanning lasers. The point sensor (not shown) draws from the front of the vehicle. As the vehicle travels, data from the point sensor and the crossed side-viewing lasers (left view) create real time gas concentration contour maps that visualize leak locations. Scanning the laser beam around the leak source provides data to quantify the leak rate.	10
Figure 2.	Standoff TDLAS.	11
Figure 3.	Previously-demonstrated Vehicle-mounted RMLD™ scanner and data illustrating robust detection of 2 scfh methane leak. Each spike represents methane detected during one revolution of the turret spinning at 120 rpm. The sensor passes through the leak plume during the 30 s period depicted.	11
Figure 4.	Sensor head with Herriot optics. Optical path length of 3 meters; physical length of 12 cm and sampling volume of 50 ml.	12
Figure 5.	Methane concentration map obtained by tomography using a scanning pair of RMLDs. Two leak sources were quantified.	12
Figure 6.	Side Scanning RMLD in fixed configuration. The commercial transceiver is further ruggedized using a PVC housing. Laser and electronic board are located inside the vehicle.	14
Figure 7.	Conical-Scan Spinning RMLD. The transceiver is enclosed in a PVC housing. Both the transceiver and the RMLD electronics were rotated when performing a scan.	15
Figure 8.	Stationary cylindrical-Scan Spinning RMLD performing cylindrical scans. This setup shows a calibrations setup with a plastic tub full of dirt and an embedded plastic tubing for calibrated gas releases.	15
Figure 9.	Methane Gas Extractive Analyzer. The major components include a pump (blue), Herriott cell (transparent tube), RMLD controller board (white square), and optical send/receive platform (black structure to the bottom right of box).	16
Figure 10.	(left) Schematic of laboratory prototype Quantitative Gas Imager; (right) Photograph of benchtop transceiver, showing OAP for light collection on the top, dual-stage scanner on the right, and laser fiber mount with collimator attached.	17
Figure 11.	Optical Methane Detector (in blue).	18
Figure 12.	Detecto Pak-Infrared (DP-IR™).	18
Figure 13.	Gasurveyor 700 Multi-Gas Detector and plunger bar to perforate ground (right).	19
Figure 14.	(left) Notional example data of methane concentration as a function of angle measured by a scanning RMLD monitoring a gas leak. (right) Geometry of scanning RMLD beam intercepting a leak plume (green).	20
Figure 15.	Diagrams depicting a scenario with positive net flux (left) and zero net flux (right).	20
Figure 16.	(Top) example map of leak survey in Las Vegas. Blue lines are survey tracks. Red Circles are leak indications, and (bottom) example of chart showing measurements from the connected sensors.	21

List of Figures (Continued)

Figure 17. Instrument Notifications. Software sees instruments by order L (left – driver side) Side Scanner, C (center – tube protruding bumper), and R (right – passenger side) Side Scanner. DMD (Digital Methane Detection) is the operating mode and StdDev refers to the algorithm used behind the software.....	22
Figure 18. Quantified plume image and flux calculation scheme for a 15 scfh methane flow obtained in DoE Phase I SBIR project.	23
Figure 19. (a) Illustrative raster pattern performed by the laser on a scene of interest. (b) The same raster scan with the resultant color map. (c) The resultant color map, where each pixel color is mapped to a specific path integrated concentration (ppm-m) measurement.....	23
Figure 20. Measured versus Metered flow rates used in RMLD-QGI flux calibration.	24
Figure 21. Mobile Leak Detection System interrogating a leak source at the Edison NJ test site hosted by PSE&G.....	25
Figure 22. FLUX Mobile equipped with spinning and side-scanning RMLDs and anemometer.	26
Figure 23. Instrumentation onboard the two survey vehicles.	26
Figure 24. Advanced Mobile Unit showing two installed side scanning RMLDs and Anemometer.	27
Figure 25. An image showing the benchtop electronics inside the car and the sensor head on tripod.	27
Figure 26. (a) Spinning RMLD data acquired from a “big” blind leak. Each rotation produces approximately 270 data points (27 seconds). Flux is computed for each rotation and averaged over the six rotations seen in the data; (b) Spinning RMLD data acquired from a “small” calibration leak (2.5 cfh).....	29
Figure 27. Diagram illustrating sites A – E used in test segments 35 – 39. Three spatially-separate concurrent leak sources are labeled site A, B and C. Sites D and E are non-leaking sources.	29
Figure 28. Methane Flux measured by spinning RMLD vs flow rate measured by rotameter in line with the gas supply during campaign #2 tests.	37
Figure 29. Leak ID#4. Top: Path-Integrated Concentration vs time (each point = 0.1 s). Middle: Trigger signal indicating spinning laser is pointing North. Bottom: Wind direction measured at vehicle roof. Ppm-m displays spikes as the laser beam crosses the gas plume upon each rotation. The spikes nominally lag the trigger by 180 deg, indicating the laser is pointing South when it crosses the plume. Therefore, the plume is blowing from the North, correlating well with the measured wind direction.....	39
Figure 30. Scanning of sewer drain using the Conical-Scan Spinning RMLD.	40
Figure 31. Time series plots with data from sewer drain.....	40
Figure 32. Leak ID#8. Top: ppm-m data showing spikes indicative of leak plume. Plume spikes lag trigger by approximately 60 deg, indicating plume blows from Southwest. Wind measured at vehicle is predominantly North or East, resulting in poor calculation of flux. Mathematically modifying the wind direction to be predominantly Southwest and North (240 deg rotation) improves the calculation.....	41

List of Figures (Continued)

Figure 33.	Distribution of field measurements conducted in Las Vegas, NV (2016).....	42
Figure 34.	Sample data from fixed RMLDs during a survey trip.....	42
Figure 35.	Comparing number of alarms from RMLDs installed in Passenger and Driver sides.	43
Figure 36.	Distribution of leaks detected by two fixed RMLDs.....	43
Figure 37.	Frequency of leaks detected by both fixed RMLDs simultaneously.....	44
Figure 38.	Efficacy of extractive method in detection of leaks when compared to fixed RMLDs.	44
Figure 39.	A sequence of frames (1 Hz) collected during a 5 SCFH controlled leak scenario at the Pico Rivera, CA SoCal facility.....	45
Figure 40.	An uncontrolled, fugitive emission stemming from a hole in the lid of a water box. Sequence of images at 1 Hz.	46

List of Tables

Table 1.	Campaign #1 Data Summary	30
Table 2.	Comparison of NYSEARCH Phase I Metered Flow Rates.....	33
Table 3.	Campaign #2 Data Summary	35
Table 4.	Campaign #3 Data Summary	38
Table 5.	Accuracy and Precision Statistics for Controlled Leak Scenarios Using the RMLD-QGI	46
Table 6.	Campaign #5 Data Summary	47

1. Motivation

The August 2014 Government & Industry Pipeline R&D Forum identified **Refining/enhancing/developing leak survey technologies and methodologies to quantify detected emissions from non-hazardous leaks to prioritize for remedial action** as a top priority technology gap requiring R&D.

Prior to this and other recent projects, natural gas leak survey tools searched for pipeline leaks by measuring the local methane concentration (ppm) or the concentration integrated over the length of a line-of-sight path (ppm-m), and roughly characterized the severity of each leak based on the leak's potential as an explosion hazard. However, surveys in several US cities observed that numerous small leaks emanate from aging cast iron distribution pipelines. While not posing immediate safety hazards, these leaks release methane, a potent greenhouse gas, to the atmosphere. To evaluate the environmental impact of specific leaks, classify and prioritize repair, and facilitate quantifying greenhouse gas emissions, technologies to rapidly and cost-effectively measure the leak rate are needed. To fill this technology gap, Physical Sciences Inc. (PSI, the technology developer) and Heath Consultants Inc. (Heath, the technology commercializer and interface with end users) proposed this R&D project to advance the ability to detect low level leaks *and provide a direct measure of the leak rate*. The research integrated advanced laser-based methane detection methods with novel system deployment configurations and wind measurements to provide leak rate data in seconds during routine mobile leak surveys.

Figure 1 illustrates the system concept. The fundamental sensor technology is the commercially-proven robust near-infrared Tunable Diode Laser Absorption Spectroscopy (TDLAS), the same technology as used in the handheld pipeline leak survey product developed by PSI and now produced and sold by Heath as the Remote Methane Leak Detector (RMLD™).

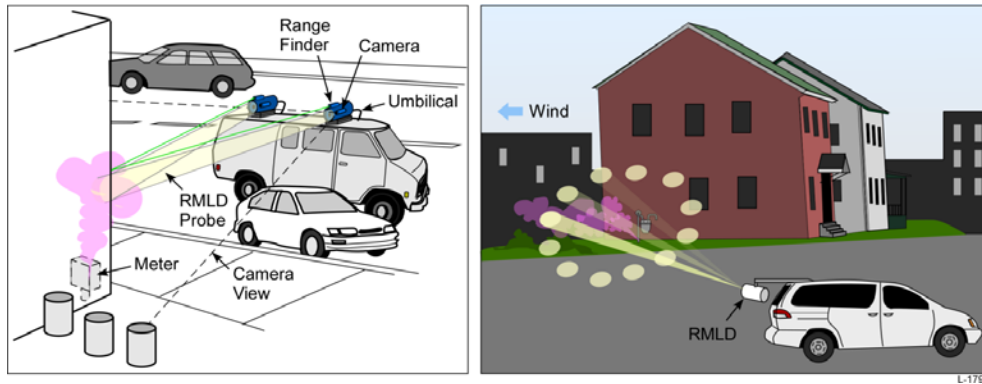


Figure 1. Mobile leak detection using combination of highly sensitive point sensors and scanning lasers. The point sensor (not shown) draws from the front of the vehicle. As the vehicle travels, data from the point sensor and the crossed side-viewing lasers (left view) create real time gas concentration contour maps that visualize leak locations. **Scanning the laser beam around the leak source provides data to quantify the leak rate.**

2. Background

Several technologies are currently utilized to detect and measure methane during routine natural gas leak surveys: e.g. gas chromatography (GC), flame ionization detection (FID), non-dispersive infrared spectroscopy (NDIR), near-IR and mid-IR tunable diode laser absorption spectroscopy (TDLAS) in various configurations including its variant cavity ring-down spectroscopy (CRDS), and infrared imaging. For leak detection, some of these technologies are incorporated into handheld tools utilized in walking surveys (e.g. RMLD™). They have been adapted to terrestrial and aerial vehicles used for mobile

surveys. Some TDLAS and CRDS sensors, incorporating multi-pass optical cells to enhance sensitivity, are deployed as sensitive single point monitors or mobile detectors. Unlike point detectors, standoff-TDLAS (utilized by RMLD™ and illustrated by Figure 2) detects very small (~5 ppm-m) methane gas leak plumes remotely, i.e. without the sensor entering the area of elevated methane concentration in the plume.

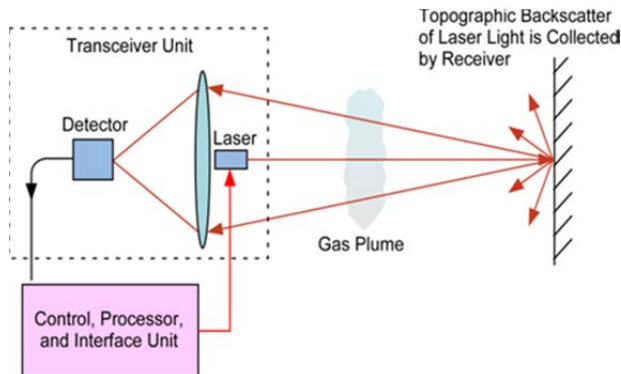


Figure 2. Standoff TDLAS.

In 2003, under DoE/NETL sponsorship, PSI deployed a prototype RMLD™ atop a vehicle from which it scanned the surrounding area via a spinning turret. Figure 3 shows the configuration and presents example data gathered as the sensor rolled above the plume 3 m downwind of a 2 scfh methane leak, illustrating sensitivity to very small leaks. As described below, the cone of laser light created by each revolution of the turret, combined with measurement of the local wind vector, provides a direct measure of the methane flux (i.e. the leak rate) emanating from within the cone.

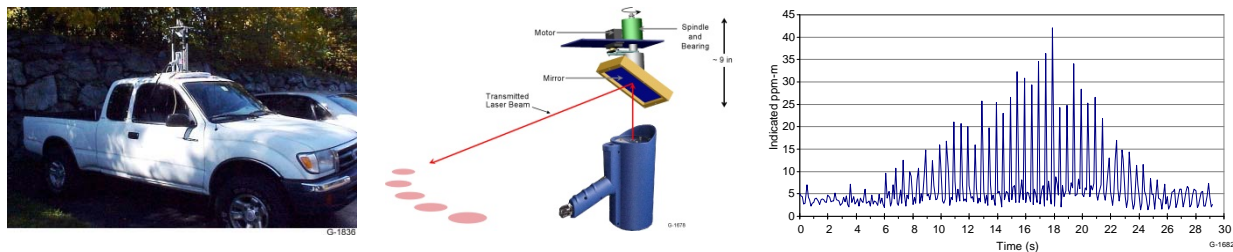


Figure 3. Previously-demonstrated Vehicle-mounted RMLD™ scanner and data illustrating robust detection of 2 scfh methane leak. Each spike represents methane detected during one revolution of the turret spinning at 120 rpm. The sensor passes through the leak plume during the 30 s period depicted.

In 2007, PSI completed projects funded by the US Department of Energy, NYSEARCH and Gaz de France to evaluate use of a side-scanned RMLD™ technology on an automobile for detecting leaks from off-street municipal pipelines. Data collected in Massachusetts and at the Gaz de France Research Facility in Paris demonstrated that a first prototype sensor detected, recorded and archived location, rate and path-integrated concentration of leaks as small as 0.7 scfh (20 l/hr) from a 30 m range, with the laser illuminating a wall surface at an elevation 50 cm above the leak source, while travelling at 40 km/hr with a modest wind blowing.

In 2010, PSI completed a Phase II SBIR project funded by the US Environmental Protection Agency to develop a sensitive TDLAS extractive (pumped) point sensor. Its sampling section achieves high sensitivity by use of a stable multi-pass optical configuration called a Herriot cell, illustrated by Figure 4. Its 0.5 ppm methane sensitivity is an order-of-magnitude better than traditional sensors commonly

deployed for mobile leak survey, but not overly sensitive to the ~0.25 ppm natural point-to-point variability of ambient methane.

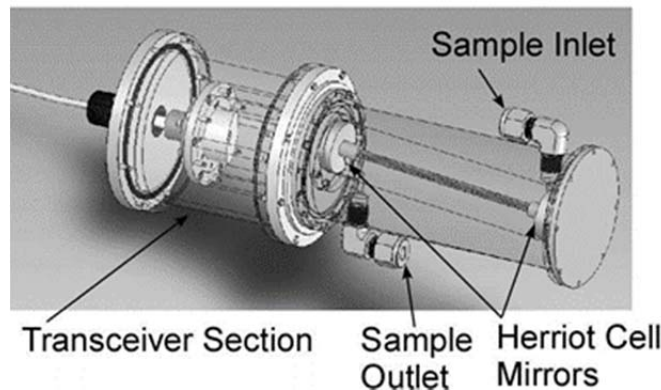


Figure 4. Sensor head with Herriot optics. Optical path length of 3 meters; physical length of 12 cm and sampling volume of 50 ml.

In 2011, the TEA-Sistemi group (Pisa, Italy) equipped a small unmanned quadrotor aerial vehicle with an RMLD™ (modified by PSI for this application) and flew a low-altitude route forming a curtain of laser light downwind of a 0.43 g/s (~85 scfh) methane leak simulating landfill emissions. Acquired data demonstrated calculation of methane flux emitted from the simulated landfill and transported by a ~3 m/s wind.

In 2013, PSI coupled a pair of RMLDs™ that scan a surface from two separate locations with tomographic inversion software to deduce a 3-d concentration profile (in ppm) of methane emitted from a leak source, specifically a simulated coal mine wall (Figure 5). When combined with a simple plume model and local wind measurement, the measured concentration can yield the methane emission rate (i.e. the flux).

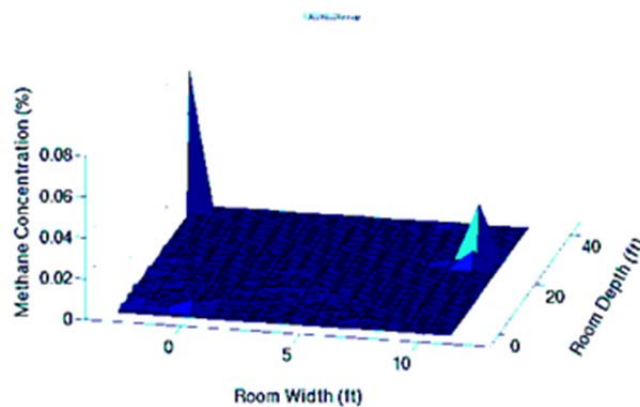


Figure 5. Methane concentration map obtained by tomography using a scanning pair of RMLDs. Two leak sources were quantified.

3. Project Objectives

The overall objective of this PHSMA R&D project was to develop survey technologies and methodologies to locate and quantify flux of non-hazardous natural gas leaks.

The successful project outcome is well documented and verified data demonstrating capabilities and limitations of the techniques, providing a foundation for subsequent leak characterization products and services.

The products and methodology for their use enable ranking leak severity to prioritize remedial actions and provide data supporting Greenhouse Gas reporting requirements.

The project objectives were met. The objectives included: (1) enhancing routine mobile leak surveys to detect and locate small leaks, and provide a rapid, cost-effective direct measure of the leak rate, and (2) evaluating and demonstrating the system as guided by a Technical Advisory Committee (TAC).

4. Project Tasks

With the inclusion of this Final Report, the nine project tasks were successfully completed. The projects tasks included:

1. Technical Advisory Committee
2. Team Meetings
3. System Hardware Development
4. Algorithms and Data Processing
5. System Integration
6. System Demonstration and Testing
7. Peer Review
8. Quarterly Progress Reports
9. Final Report

5. Task 1: Assembly of a Technical Advisory Committee (TAC)

The formation of a Technical Advisory Committee was initially suggested in the proposal. TAC was to comprise of a group of volunteers representing end users of the technology or data: pipeline operators, regulators from FERC or the States, and SME's. However, the establishment of a Methane Detection Technologies Project by the Interstate Technology Regulatory Council (ITRC) in March 2016 obviated the utility of a separate TAC.

The ITRC project team comprises more than 20 individuals representing the roles and performing the functions initially envisioned for the TAC. The ITRC team includes Jim Rutherford of Heath Consultants, the commercial partner of this PHMSA project. Via monthly conference calls and other meetings, the team has discussed technologies with a view towards developing future standards for vehicle-based mobile leak surveying and quantification.

A common theme in these discussions is recognition that emerging technologies which distinguish natural gas from other methane sources (e.g. biogas emitted by swamps, sewers, landfills, etc.) are desirable for mobile surveys, particularly for discriminating against false detections of gas leaks. This guidance led PSI and Heath to consider including such capability as part of this PHMSA project. An example is the concurrent measurement of both methane and ethane, ethane being a component of natural gas but not biogas. As described in the quarterly reports, PSI discussed the importance of this dual-gas measurement system with PHMSA. New hardware to address this need was not developed in this project as this is

beyond the scope of the proposed work. However, Heath has now integrated a commercial extractive ethane/methane analyzer into their advanced mobile survey vehicle.

6. Task 2: Team Meetings

Project team meetings were conducted to review project goals and progress. The first one was the Kick-off Meeting held on December 2015. Frequent team meetings were conducted during the duration of this project.

7. Task 3: System Hardware Enhancements

The commercial methane sensor, RMLD, was incorporated into vehicles in a fixed or spinning configuration (conical or cylindrical scan setup) as well as in handheld configuration. The use of these sensors allowed focus on field measurement campaigns rather than sensor development. Additional hardware included the multi-pass gas analyzer and the newly developed first ever field-deployed gas leak rate imager. The following sections describe each of these technologies in detail. System integration into the survey vehicles is described in Section 9.

Side Scanning RMLD

The Side Scanners are RMLD-IS transceivers mounted on the roof rack, see Figure 6. One unit aimed to the vehicle's left, the other to the right. The side scanning RMLD continuously collected data while the vehicle was moving within the local speed limit. The commercial RMLD transceiver was ruggedized (using PVC housing) for storage in all weather conditions. The electronics and laser units were located inside the vehicle. The transceiver was fixed in position typically oriented about 10 degrees (from center) toward the front of the vehicle and aimed slightly downward for its laser beam to intercept the road surface nominally 30 ft distant.



Figure 6. Side Scanning RMLD in fixed configuration. The commercial transceiver is further ruggedized using a PVC housing. Laser and electronic board are located inside the vehicle.

Spinning RMLD

Two versions of the spinning RMLD were designed and deployed during the course of this project: 1) an adjustable conical scanner mounted to the vehicle roof; and 2) a portable (tripod-mounted) cylindrical scanner. Data were collected while the vehicle was stationary.

Conical-scan spinning RMLD is mounted from the roof on a motorized platform, see Figure 7. It aims towards the ground. The angle of the axis-of-rotation relative to the ground was adjustable, as was the angle of the RMLD transceiver relative to the axis-of-rotation. A typical configuration circumscribed an elliptical laser path around the leak source with a major axis of approximately 5 ft. while the vehicle was stationary. The entire RMLD unit spun at a rate of two rotations per minute. It was equipped with a sensor

(“trigger”) that signaled the start of each rotation and located the orientation of the transceiver relative to the wind. The unit continuously and wirelessly transmitted data to the recording and data processing software. The non-vertical conical shape obtained from the spinning motion complicated analysis and introduced error as cross-section changes with azimuth and direction. Furthermore, variable wind direction and speed introduced error.



Figure 7. Conical-Scan Spinning RMLD. The transceiver is enclosed in a PVC housing. Both the transceiver and the RMLD electronics were rotated when performing a scan.

Cylindrical-scan spinning RMLD was found to be preferable and less sensitive to wind and height. Faster scans are better than slow ones to accommodate wind variability. The downward-facing RMLD mounts at the end of a camera jib arm elevated approximately 5 ft above ground, see Figure 8. The arm was attached to a tripod via a motor-controlled turntable. A counterweight hung on the opposite end of the arm. When spinning, the RMLD beam traced a 7.5 ft diameter circle on the ground around the turntable axis. Rotation rate was set at 6 rpm. A trigger signal indicated the start of each rotation, corresponding to the arm pointing North. A personal computer recorded data points at 10 Hz, i.e. 0.1s per point, nominally 100 points per rotation. A sonic anemometer attached to the tripod provided wind speed and direction updated every second. The analysis software utilized wind speed, direction, and RMLD measurement of ppm-m to compute methane flux for each rotation. It averaged the values from ten rotations for each output result. This platform provided data to validate the scanning approach for measuring leak rates without geometrical complications from the conical-scan approach that requires additional corrections.



Figure 8. Stationary cylindrical-Scan Spinning RMLD performing cylindrical scans. This setup shows a calibrations setup with a plastic tub full of dirt and an embedded plastic tubing for calibrated gas releases.

Extractive Gas Analyzer

Methane analyzers (i.e. point sensing) onboard vehicles are commonly used in surveys of urban areas to identify leaks. A TDLAS analyzer designed and built by PSI was incorporated into a survey vehicle and results were compared to open-path sensors.

Figure 9 shows a CAD drawing of the PSI extractive gas analyzer highlighting the major components. The analyzer measurement volume was based on a Herriott cell design having two concave cylindrical mirrors with prescribed focal length and separation distance to generate a total optical path length of 10 meters. A RMLD controller board was incorporated for laser control and data acquisition. A pump continuously drew gas samples from the front of the vehicle during operation. This analyzer was installed inside the vehicle with a sampling tube located in front-center of the vehicle. The detection limit is 0.5 ppm at 1Hz bandwidth. The instrument alarm threshold was set at 10x the detection limit, 5 ppm.

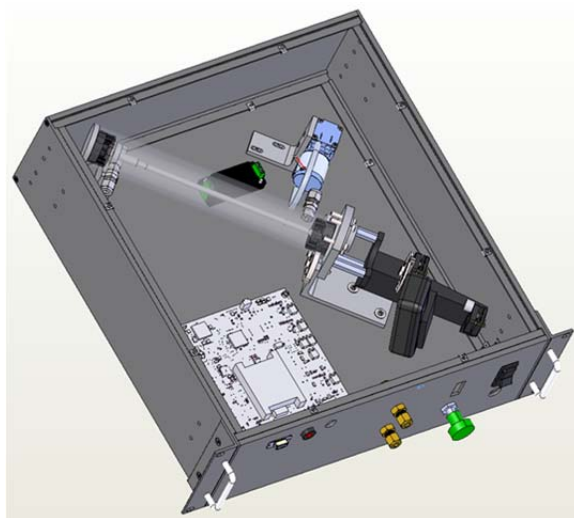


Figure 9. Methane Gas Extractive Analyzer. The major components include a pump (blue), Herriott cell (transparent tube), RMLD controller board (white square), and optical send/receive platform (black structure to the bottom right of box).

Gas Imager (RMLD-QGI)

This project originally envisioned deploying two roof-mounted RMLD units to obtain data suitable for tomographic inversion to deduce leak rates. Further consideration of this technique led to the conclusion that, because it required a two-dimensional scan from a moving vehicle coupled with remote wind measurement, it would be impractical to develop and implement within the context of this project. Instead, we tested a preferred leak identification, imaging, and quantification technique that evolved from the earlier spinning-RMLD techniques described above. During the course of this project, the early work was complemented by a DoE-funded Phase I SBIR project wherein PSI demonstrated a novel scanning RMLD system that created a quantified two-dimensional image of a methane leak plume and named the “Quantitative Gas Imager (QGI)”. The image contained information from which plume flux can be deduced. Specifically, the flux algorithm selects from the image a set of pixels that surround the leak source and then deploys the same flux calculation method as with the spinning RMLD in the cylindrical-scan configuration that created a laser “curtain” circumscribing the leak source.

Figure 10 illustrates the components of the tabletop QGI. The handheld transceiver depicted on the left was replaced with breadboard components pictured on the right. The components included a two-stage

galvo scanner for laser scanning the scene, laser beam launch mount with a collimator, and off-axis parabolic mirror collecting the backscattered light and focusing it onto the detector. A simple video camera was attached to this setup to image the scene and superimposed the measured concentration of methane in the scanned field. This near real-time visualization of the imaged leak on a laptop screen was essential during the field tests. This apparatus was packaged for vehicle deployment and field tested with complementary funds from NYSEARCH and test site provided by SoCal in the neighborhood of Pico Rivera, CA.

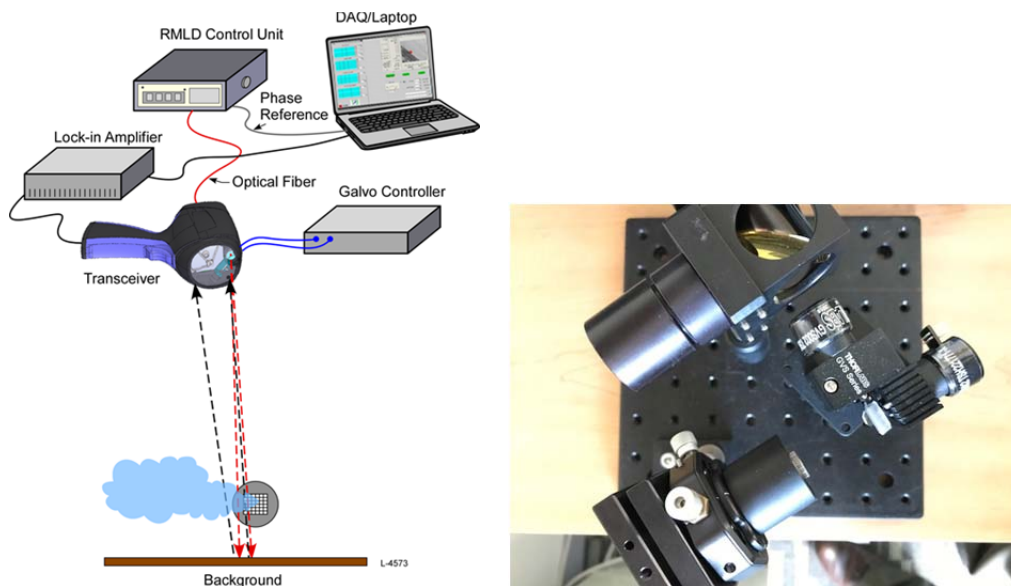


Figure 10. (left) Schematic of laboratory prototype Quantitative Gas Imager; (right) Photograph of benchtop transceiver, showing OAP for light collection on the top, dual-stage scanner on the right, and laser fiber mount with collimator attached.

Other Hardware Enhancements Using Commercial Sensors

*Optical Methane Detector (OMDTM)*¹, Figure 11, uses advanced infrared technology to conduct mobile inspections of buried natural gas distribution, transmission, and gathering pipelines. This is a commercial product offered by Heath and supplemented our suite of sensors. The OMD was front mounted on a vehicle and calibrated by the driver or technician from inside the vehicle eliminating potential hazards such as explosive calibration gases. Leak indications were both audible and visual from inside the vehicle. Data can be sent to a data logger or translated to a ground positioning satellite (GPS) system. Adding-on the Heath Survey Tracker (improved in this project using an existing software) allows the ability to log mobile leak survey data and GPS locations of all natural gas leaks detected.

¹ <http://heathus.com/products/optical-methane-detector-omd/>



Figure 11. Optical Methane Detector (in blue).

Detecto Pak-Infrared (DP-IRTM)² sensor was also used to pinpoint the leak in addition to the RMLD in some of the surveys. Figure 12 shows the device configuration in typical operation in the field. This was developed by Heath to replace the current surveying equipment that uses the flame ionization technique. The detection method is based on infrared controlled interference polarization spectrometer. The sensor operates by drawing continuous samples using a handheld probe. Upon locating the hot spot, the probe was left touching the surface to identify the highest reading. Readings were taken at surface and 2 inches above the ground. Surface spread was determined by moving the DP-IR around the hot spot until a zero reading was obtained. The locations of the zero readings and hot spot were used to determine the surface spread of the leak.



Figure 12. Detecto Pak-Infrared (DP-IRTM).

² <http://heathus.com/products/detecto-pak-infrared/>

Gasurveyor 700 (GS700)³, a commercial product sold by Heath is used to determine ground spread of a leak once the leak is pinpointed by the RMLD or DP-IR. A plunger bar was used to perforate the ground around the hot spot location until the GS700 gave a zero reading. GS700 is based on the latest infrared gas detection technology in a robust and reliable design with data-logging and GPS mapping. Figure 13 shows a photograph of the sensor (left), probe connected to sample around a man-hole cover (center), and a plunger in action (right).



Figure 13. Gasurveyor 700 Multi-Gas Detector and plunger bar to perforate ground (right).

8. Task 4: System Data Processing and Algorithms Development

The methods to compute fluxes from the spinning RMLD in both cylindrical and conical-scan configurations are discussed. The software and GUI for tracking the leak surveys were improved building on the existing software. Data processing algorithm for the leak rate imager is also presented.

Computing Flux from Conical-Scan Spinning RMLD

Figure 14 illustrates an example sensing scenario. The RMLD beam is directed sideways toward a target at range h from the vehicle. The beam scans an angle θ around the centerline, circumscribing the leak source at radius r . Wind blows the plume through the cone as shown. Along the surface of this laser light cone, the RMLD measures the integrated column density. Figure 14-left presents notional data detected during the 360 degrees conical scan of the laser beam around the source. As the beam sweeps through the plume, the signal increases above the ($\sim 2 \text{ ppm} * 3 \text{ m standoff} = 6 \text{ ppm-m}$) background.

The net flux of methane flowing through the surface of the cone is

$$\dot{m} = \int_0^{2\pi} \bar{u} \cdot \bar{r} \left[\int_0^H \rho(r, \theta, h) dh \right] d\theta \quad (1)$$

where u is the wind vector and ρ the methane concentration at coordinates r, θ, h . The term $\int_0^H \rho dh$ is the methane column density (i.e. path-integrated concentration) measured by RMLDTM. Leakage from within the cone yields a non-zero net methane flux (i.e. the leak flow rate). Any methane flowing through but not originating within the cone yields zero net flux (assuming constant and uniform wind within the cone). *Preliminary performance estimates indicate that the method can measure the flux from a nominal 2 scfh leak in a 3 m/s wind in less than 10 s with accuracy (standard deviation) better than 20%.*

³ <http://heathus.com/products/gasurveyor-700/>

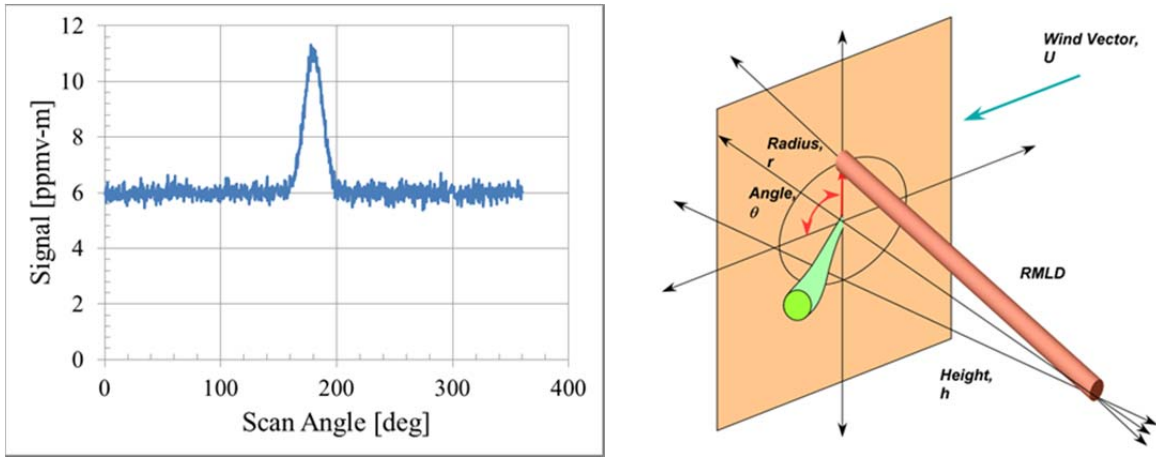


Figure 14. (left) Notional example data of methane concentration as a function of angle measured by a scanning RMLD monitoring a gas leak. (right) Geometry of scanning RMLD beam intercepting a leak plume (green).

Computing Flux from Cylindrical-Scan Spinning RMLD

The area of interest is encircled by using a cylindrical-scan spinning RMLD with laser light projected to the ground from above, providing a simpler analysis than the conical configuration. The net methane flux flowing through each cylinder = (column-integrated concentration measured by RMLD) * (cylinder cross section) * (wind speed). Only methane emitted from within the cylinder yields a non-zero net flux; methane originating from outside but passing through the cylinder yields zero net flux, as illustrated in Figure 15. These attributes make the scanning RMLD an inherent localizer of leak sources.

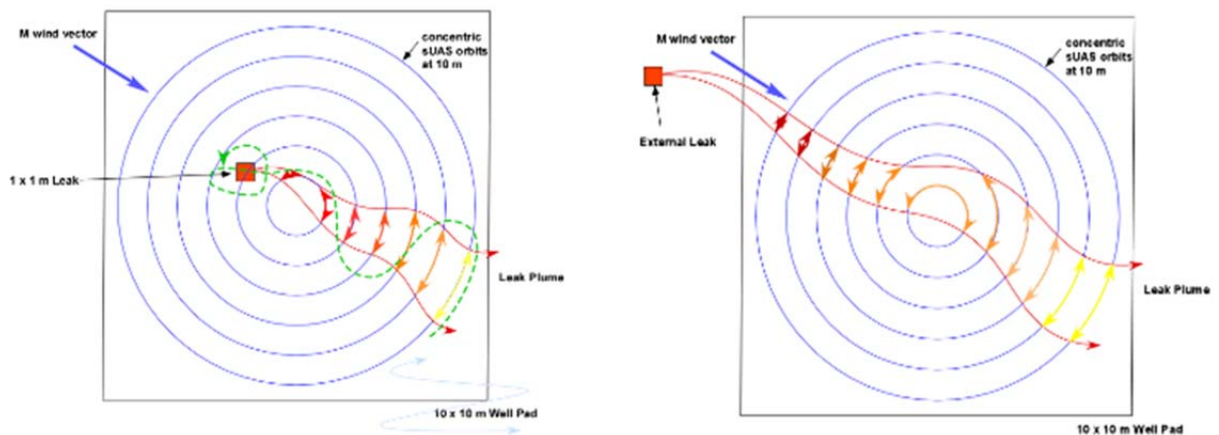


Figure 15. Diagrams depicting a scenario with positive net flux (left) and zero net flux (right).

GUI for Data Acquisition, Display and Reporting

The graphical user interface (GUI) and software for tracking and annotating all conducted surveys were instrumental to this project. This developed software is now incorporated into Heath's MobileGuard™ – an advanced vehicle leak detection system that also incorporates a methane/ethane analyzer, GPS, and a sonic anemometer to estimate the leak location. Top of Figure 16 shows an example of the map with tracked routes with annotated locations and sensor outputs. The location does not pinpoint the origin of the leak, but the GPS location of when the instruments detected gas. There is about 6-7 second delay for

the instrument to read gas. Concentrations recorded by the two fixed-position RMLDs (in ppm-m) and analyzer (in ppm) are accessible from the tab labeled “Chart.” The side scanners have a manual min/max scale. The legend at the right corner of window explains RMLD color code and it follows software order of instruments: Left (driver side) Side Scanner (CGI#1), Center (CGI#2), and Right (passenger side) Side Scanner.

When an instrument detects a gas level exceeding threshold, notifications are displayed on the map. The software will display one or more of the images presented in Figure 17, identifying which instrument detected gas. Software sees instruments by order L (left – driver side) Side Scanner, C (center – tube protruding bumper), and R (right – passenger side) Side Scanner. DMD is the operating mode and StdDev refers to the algorithm used behind the software. A detailed manual describing the functions of this advanced data logger was attached to Quarterly Report No. 4.

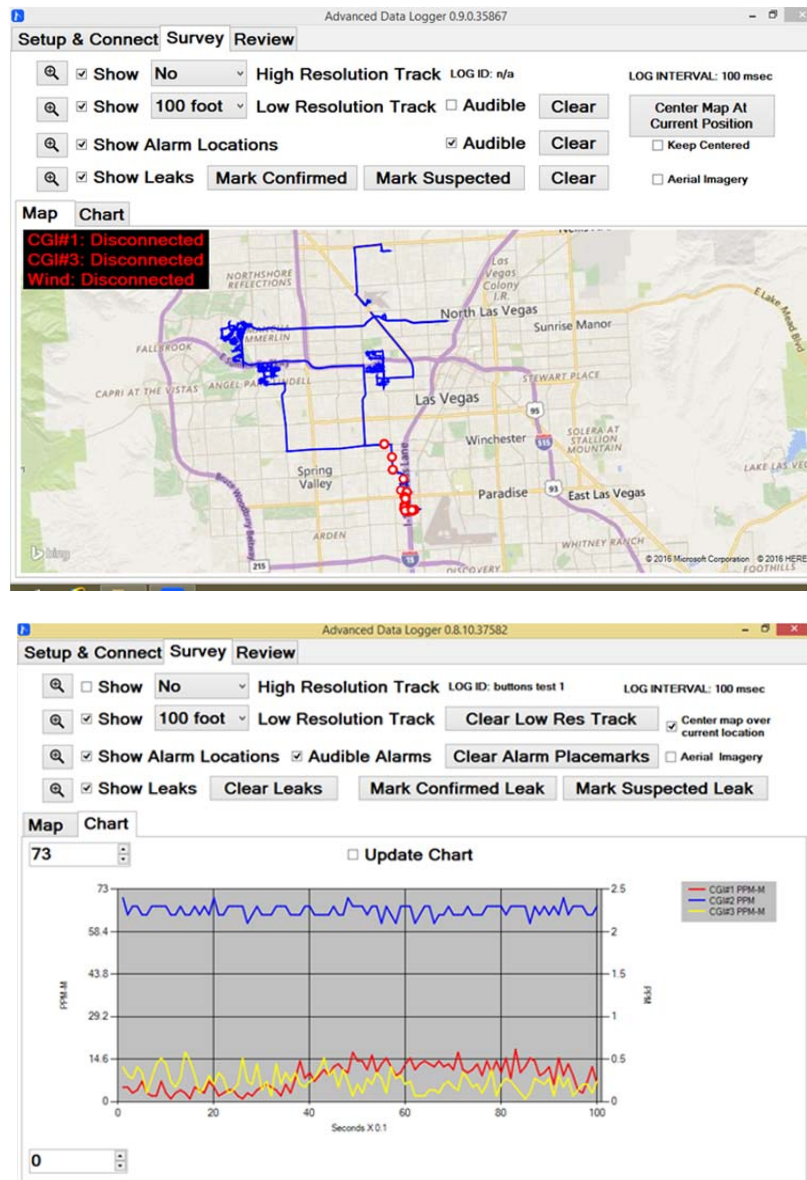


Figure 16. (Top) example map of leak survey in Las Vegas. Blue lines are survey tracks. Red Circles are leak indications, and (bottom) example of chart showing measurements from the connected sensors.



Figure 17. Instrument Notifications. Software sees instruments by order L (left – driver side) Side Scanner, C (center – tube protruding bumper), and R (right – passenger side) Side Scanner. DMD (Digital Methane Detection) is the operating mode and StdDev refers to the algorithm used behind the software.

Data Processing for RMLD-QGI

Using novel algorithms developed in conjunction with other R&D projects at PSI⁴, the plume flux (i.e. emission rate) emanating from the interrogated area is deduced as follows.⁵ The flux of gas, Q , having concentration $c(x, y, z)$ (ppm) flowing with velocity $u(x, y, z)$ through a surface S located a distance x_o downwind of a source (e.g. Figure 5) is:

$$Q = \int_S c(x_o, y, z) u(x_o, y, z) ds \quad (1)$$

where

$$\int_S c(x_o, y, z) u(x_o, y, z) ds = \int_{-W}^W dy \int_0^H c(x_o, y, z) u(x_o, y, z) dz \quad (2)$$

and W and H are the lateral and vertical dimensions of the plume wherein $c > 0$. Estimating the flow velocity (i.e. wind) as uniform \hat{u} across the surface yields

$$\int_0^H c(x_o, y, z) u(x_o, y, z) dz = \hat{u}(x_o) \int_0^H c(x_o, y, z) dz \quad (3)$$

and thus

$$Q = \hat{u}(x_o) \int_{-W}^W \langle c(x_o, y) \rangle dy \quad (4)$$

where $\langle c(x_o, y) \rangle$, the vertical (z -direction) path-integrated column concentration (ppm-m) at horizontal location y , is measured directly by the RMLD laser beam. Because the quantified plume images produced by the scanned laser beam of our novel imaging instrument contain the $\langle c(x_o, y) \rangle$ information, Q is deduced by measuring $\langle c(x_o, y) \rangle$ vs y and using an estimated wind speed \hat{u} . Wind speed is measured with a supplemental wind sensor, or may be determined by measuring plume motion in successive images. Software selects a representative surface S through which the imaged plume crosses. The surface may be depicted as a line in the imaged scene (i.e. a laser-delineated plane through which the plume crosses (Figure 18)), or a circle or other shape circumscribing the emission source.

⁴ Frish, M.B., Wainner, R.T., Green, B.D., Laderer, M.C., and Allen, M.G., “Standoff Gas Leak Detectors Based on Tunable Diode Laser Absorption Spectroscopy,” SPIE Paper No. 6010-13, Optics East, Boston, MA, 23-26 October 2005.

⁵ Frish, M.B., “Methane Leak Surveying with Small Unmanned Aerial Systems”, CH4 Connections 2015 Workshop, The Woodlands, TX, PSI VG-2015-111, October 2015.

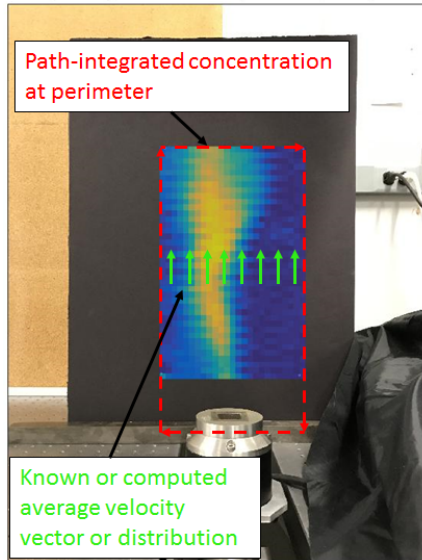


Figure 18. Quantified plume image and flux calculation scheme for a 15 scfh methane flow obtained in DoE Phase I SBIR project.

Figure 19 illustrates the flux calculation concept as applied to the RMLD-QGI scenario. The figure illustrates a vertical plume which, in reality, is more likely to be horizontal carried by the wind. Also ideally, as illustrated, the TDLAS mapping would encompass the source (this helps by cancelling out any global ambient methane concentration). The calculation is performed by integrating the vector product of the TDLAS data (ppm-m) with the local velocity vector (m/s). This velocity is to be either (a) user input from a known current wind value, (b) recorded from a local portable anemometer, or (c) deduced via a velocimetry algorithm / mode from the RMLD-QGI data itself. Note that the vertical edges in this example contribute zero as they are parallel to the flow vector. In order to create the quantified color map, the laser is rastered through the scene as shown in Figure 19a. The resultant image with color proportional to concentration is shown in Figure 19c.

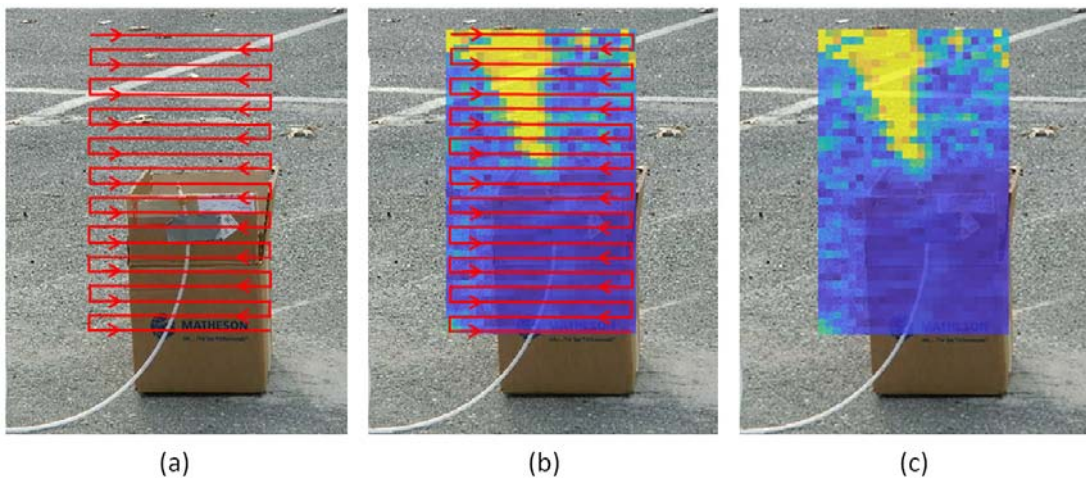


Figure 19. (a) Illustrative raster pattern performed by the laser on a scene of interest. (b) The same raster scan with the resultant color map. (c) The resultant color map, where each pixel color is mapped to a specific path integrated concentration (ppm-m) measurement.

Post-processing algorithms were developed to generate these color maps and estimate leak rate. The current algorithm examines the distribution of a single frame of ppm-m data. Data points within the frame are isolated as either leak/plume contributors or background. Subtracting background from plume contributions, factoring in wind intensity and applying a calibration factor provides an estimated flux. Figure 20 below shows the calibration results for five controlled leak scenarios, and the expected precision and accuracies of the system for this range of flow rates.

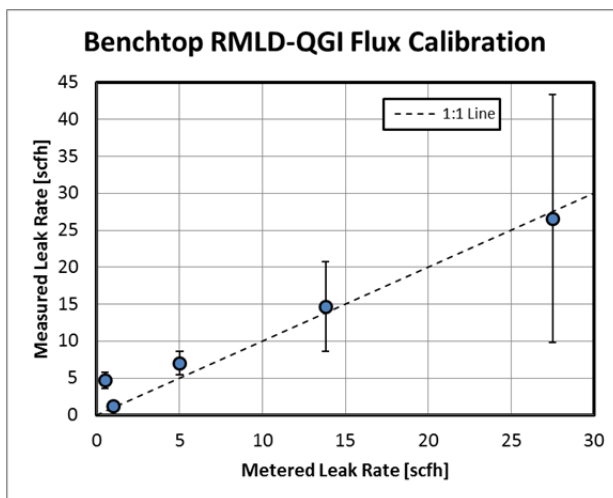


Figure 20. Measured versus Metered flow rates used in RMLD-QGI flux calibration.

As can be seen in Figure 20, it is apparent that the precision of the flux estimates decreases with increased flow rate. It is worth noting that accuracy is maintained, however, indicating that a sufficient number of frames of data should be acquired in order for averaging to converge to an accurate flux estimate. For all tests, at least 10 seconds of data are acquired (at 1Hz frame rates).

9. Task 5: System Integration

In this Task 5, the hardware described in Task 3 (Section 7 above) was integrated into several platforms suitable for specific measurement campaigns including both controlled and real-world leak scenarios. These platforms included (1) a vehicle equipped with conical-scan spinning RMLD and other sensors, (2) the FLUX-Mobile with conical-scan spinning RMLD with adjustable aim, (3) Advanced Mobile Units comprised of two vehicles fitted with an array of sensors including a methane analyzer, and (4) RMLD-QGI for 2D imaging leak rate detection with processing electronics housed onboard a vehicle.

Mobile Leak Detection System

The mobile system as shown in Figure 21 included: 1) a spinning RMLD, mounted on the roof, that creates a laser light cone around a leak source to quantify leakage rates 2) a fixed-aim side-viewing RMLD, also mounted on the roof; 3) extractive sensors, installed within the vehicle, that draw gas via tubing having inlets at the front of the vehicle; and 4) an anemometer mounted on the roof. In addition, a handheld RMLD unit and a Heath DP-IR unit acquired supplemental independent data during the tests.

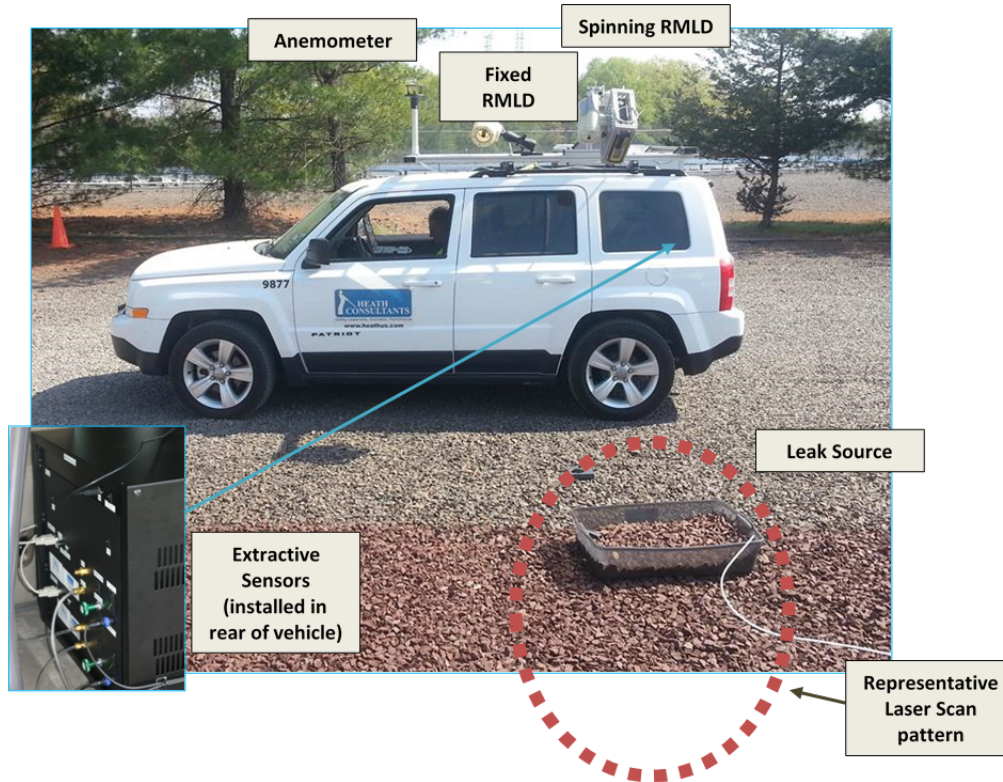


Figure 21. Mobile Leak Detection System interrogating a leak source at the Edison NJ test site hosted by PSE&G.

The first evaluation of leak rate quantification using the spinning RMLD sensor was conducted in conjunction with a field test hosted by NYSEARCH member PSE&G. This sensor operated with the vehicle stopped in close proximity to the leak source while the RMLD laser beam scans a cone enfolding the source. Along the surface of this laser light cone, the RMLD measured the integrated column density.

For each test, the mobile system was parked in a position such that the laser cone of the spinning RMLD encircled the leak source. Data were collected for 6 – 10 revolutions around the leak source, measuring ppm-m along the laser path at a rate of 10 points per second. Each rotation required approximately 27 seconds, thus the data collection period was approximately 3 – 5 minutes. DP-IR and handheld RMLD measurements were collected at most sites for reference only. Approximately 15 – 20 minutes total time was required at each measurement site, including parking the vehicle, installing obstructions, setting flow rate, acquiring handheld sensor measurements, and finally acquiring spinning RMLD data and writing notes.

FLUX Mobile

Figure 22 shows a photograph of the FLUX Mobile incorporating 1) a spinning RMLD with conical-scan configuration, mounted on the roof, that creates a laser light cone around a leak source to quantify leakage rates 2) a fixed-aim side-viewing RMLD, also mounted on the roof; 3) an anemometer mounted on the roof; 4) a GPS; and 5) monitoring, processing, recording, and mapping software operating on a Windows laptop. The entire system is powered by the vehicle's battery.



Figure 22. FLUX Mobile equipped with spinning and side-scanning RMLDs and anemometer.

The FLUX Mobile is driven around until a leak is detected. The vehicle stopped at the identified leak location and performed scans of the area. The scanned measurements were processed and a leak rate in scfh was computed.

Advanced Mobile Unit

Two survey vehicles were equipped with several sensors as illustrated in Figure 23. The lead car was instrumented with one optical methane detector (OMD) in the front and with two technicians holding a remote methane leak detector (RMLD) each. The trailing advanced mobile car had two fixed RMLDs mounted on top of the car (Figure 24). The Herriott cell extractive analyzer (HC) was installed in the back of the vehicle and sample gas was drawn from the front-center of the vehicle. Distance between the two cars was maintained between 2 – 3 (typical) vehicle-lengths apart and at most 10.

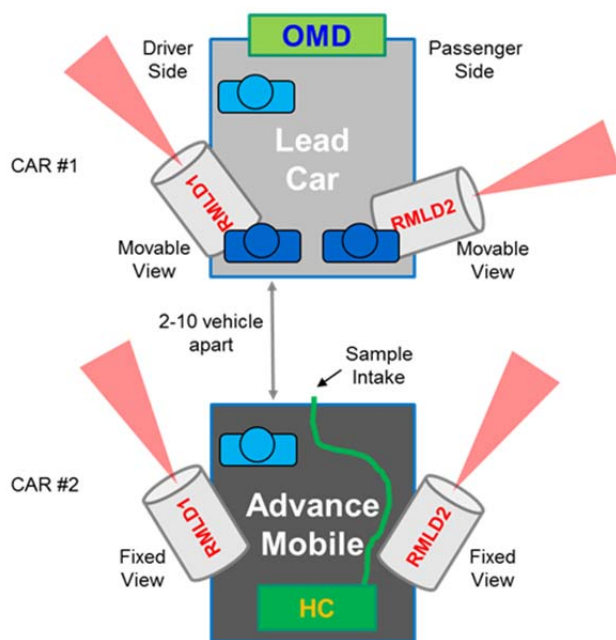


Figure 23. Instrumentation onboard the two survey vehicles.



Figure 24. Advanced Mobile Unit showing two installed side scanning RMLDs and Anemometer.

In a typical survey mission, the two vehicles were dispatched. While the vehicles were moving, the fixed and handheld RMLDs continuously scan the sides of the road, the analyzer sampled the incoming air, and the OMD sampled the path of air in front of the Lead Vehicle. Data from the fixed RMLDs and analyzer are recorded at 10Hz. In some leak scenarios that required further inspection, the RMLD and DP-IR were used to locate the hot spot. Other commercial sensors were used to determine the surface and ground spread of the identified leaks.

RMLD-QGI Field Prototype

Figure 25 shows a photograph of the setup of the field prototype RMLD-QGI. The benchtop electronics were located inside the car and comprised of RMLD driving electronics, benchtop current pre-amplifier, benchtop signal lock-in amplifier, and high-speed data acquisition system.

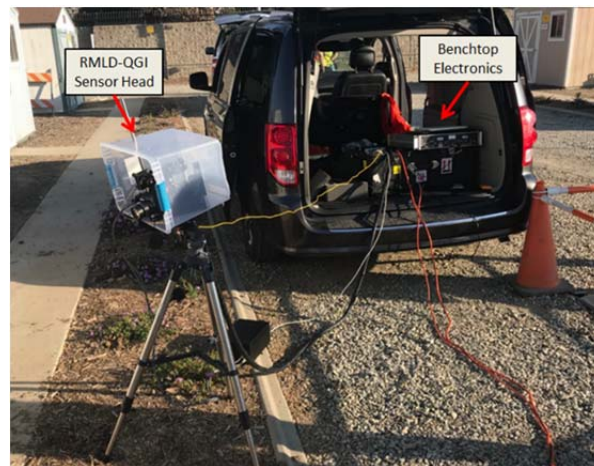


Figure 25. An image showing the benchtop electronics inside the car and the sensor head on tripod.

Because of the nature of a benchtop laboratory prototype, there were a few system constraints. The major constraint was transportability. The system was tethered to a transporting vehicle. Thus the prototype system was best suited for measurements on sidewalks, parking lots, or other areas accessible by vehicle. This tether existed due to a need of AC power from the inverter-equipped vehicle, and benchtop electronics. Additionally, the system was not yet weatherproofed, therefore could not operate during times

of precipitation. These constraints will be addressed in future generations of the technology. The system can operate with and without cloud cover, but does need a direct line-of-sight with the leak in order to operate effectively.

In this project, the RMLD-QGI was brought to previously identified hot spots with the main function of determining the leak rates. Knowledge of leak rates is useful in prioritizing leaks for repairs. The user placed the sensor head approximately 10ft away from the leak source and aimed the head appropriately. The benchtop electronics were configured and the data collection exemplified in Figure 19 then commenced. In conjunction with this data, anemometer measurements were made. By measuring path integrated concentrations (ppm-m) from the RMLD-QGI, and wind speeds and directions, all data required to estimate leak rate were available.

10. Task 6: System Demonstration and Testing

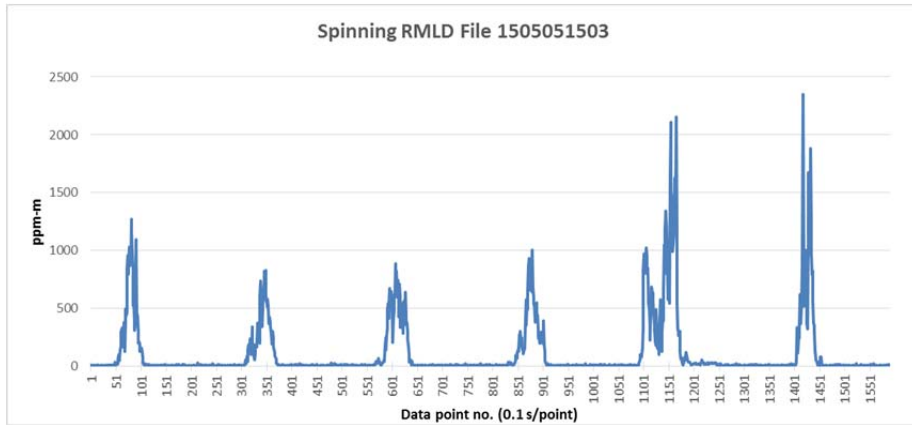
Many opportunities for field tests were made available during this project to demonstrate and validate the instruments in real world leak scenarios. Several field test campaigns were conducted using the fixed and spinning RMLD configuration, as well as the first-ever demonstration of the leak rate imager. A total of five field test campaigns were conducted with sensor configurations and field test locations summarized below:

- Campaign #1: collected 72 data files covering a range of conditions at the PSE&G test site in Edison, NJ. Conical-scan spinning RMLD used.
- Campaign #2: collected 173 data files covering a range of conditions spreading over 84 distinct tests at the SolCal test site in Commerce, CA. Cylindrical-scan spinning RMLD used
- Campaign #3: investigated 15 locations in Westchester County, NY, near the ConEd facility in Elmsford, NY. Conical-scan spinning RMLD with remotely adjustable aim was used.
- Campaign #4: conducted over 400 survey sorties in Las Vegas, CA. Utilized two vehicles with fixed and handheld RMLDs, analyzer, and a number of other commercial sensors.
- Campaign #5: conducted 51 tests in municipal settings located in Pico Rivera, CA. RMLD-QGI was used.

Campaign #1: Stationary Conical-Scan Spinning RMLD

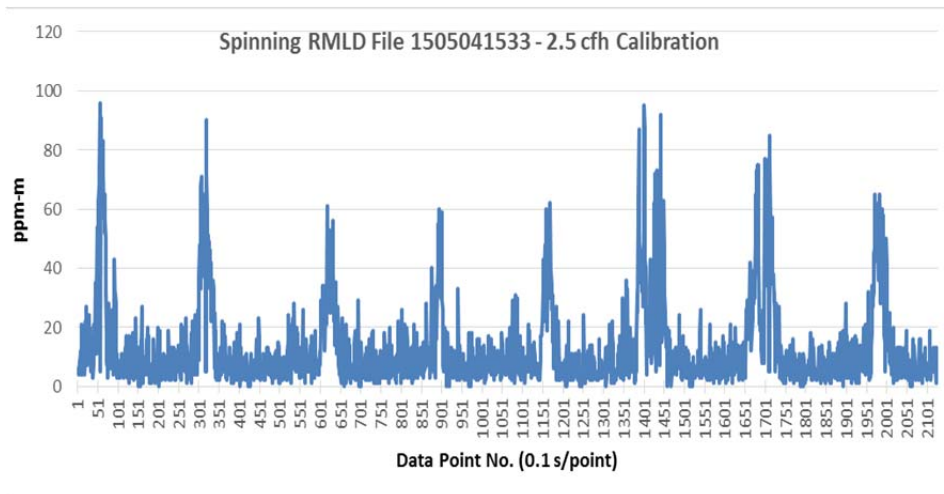
A total of 72 data files were collected spanning various test configurations following NYSEARCH Phase I Test Plan. These tests (manufactured leaks) were used to evaluate the leak rate quantification using the spinning RMLD sensor. Of these, all but six were “blind” measurements wherein the flow rate was unknown to the measurement team. Six measurements were made for “calibration”; these measurements differed from others only in that the actual flow rate was reported by NYSEARCH to the team. Figures 26a and 26b show example data sets.

Table 1 summarizes the test data collected at the various sites and configurations defined in the NYSEARCH Test Plan, and accompanying Figure 26 describes the test sites A - E. For Test Segments 35-39, having three spatially-separate concurrent leak sources, Sites D and E are locations between two leak sources, and Site F is downwind of the three leaks. Algorithms for processing and analyzing data were not available for real-time results during data acquisition. The algorithms were implemented to post-process the acquired data.



Points	Adjusted Flux (cfh)
1-268	59
269-536	47
537-804	58
805-1072	55
1073-1340	110
1341-1589	71
Average	67
std dev	22

(a)



Points	Adjusted Flux (cfh)
1-268	2.9
269-536	2.7
537-804	1.8
805-1072	1.3
1073-1340	1.4
1341-1608	3.1
1609-1876	3.4
1877-2024	2.8
Average	2.42
Std Dev	0.82

(b)

Figure 26. (a) Spinning RMLD data acquired from a “big” blind leak. Each rotation produces approximately 270 data points (27 seconds). Flux is computed for each rotation and averaged over the six rotations seen in the data; (b) Spinning RMLD data acquired from a “small” calibration leak (2.5 cfh).

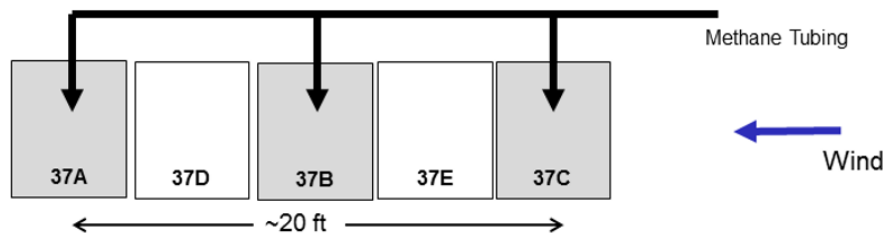


Figure 27. Diagram illustrating sites A – E used in test segments 35 – 39. Three spatially-separate concurrent leak sources are labeled site A, B and C. Sites D and E are non-leaking sources.

Table 1. Campaign #1 Data Summary

Segment #	Time	location	blockage	Wind Direction	Wind Speed	Comment	manual observation	Method 1 DPIR+RMLD Est cfh	Method 2 Spinner Avg. Est cfh	Method 3 Spinner Calculated cfh (avg)	Method 3 Spinner Calculated cfh (std dev)	Spinner Calc Class
10 cfh calibration	05041513	a3	none	250 +/- 40	3 +/- 3				10	10.5	5.3	medium
2.5 cfh calibration	05041533	a3	none	250 +/- 40	3 +/- 3				3	2.4	0.5	small
0.8 cfh calibration	05041556	a3	none	250 +/- 40	3 +/- 3				2	2.1	1	small
0.2 cfh calibration	05041608	a3	none	250 +/- 40	3 +/- 3				0.5	0.9	0.3	small
4	05041634	a3	none	270 +/- 40	3 +/- 3		small	13.8	3.5	1.3	0.8	small
5	05041654	a3	none	270 +/- 40	3 +/- 3		tiny	3.5	0.1	0	0.8	small
6	05041710	a3	prf dwn wind	270 +/- 40	3 +/- 3		medium-big	132.5	33	43.1	17	big
7	05041720	a3	solid dwn wind	270 +/- 40	3 +/- 3		huge	203.2	100	71.8	47.5	big
8	05041740	a3	Prf up wind	270 +/- 40	3 +/- 3			40.4	15	9.9	3.3	small
9	05041755	a3	solid up wind	270 +/- 40	3 +/- 3			6.9	14	15.3	5.6	medium
50 cfh calibration	05050810	a3	none	300 +/- 50	2 +/- 1				50	51.3	21.6	big
10 cfh calibration	05050830	a3	none	300 +/- 50	2 +/- 1	out of gas near end?			9.5	8.3	5.5	small
10	05051340	b7	none	300 +/- 50	2.5 +/- 2.5		very small	2.8	0.1	0.5	0.4	small
11	05051350	b7	none	300 +/- 50	2.5 +/- 2.5		medium - big	99.3	17.5	10.7	4.3	medium
12	05051405	b7	prf dwn wind	300 +/- 50	2.5 +/- 2.5		medium	28.1	16	8.7	5.9	small
13	05051412	b7	solid dwn wind	300 +/- 50	2.5 +/- 2.5		big	187.3	112	65.7	54.9	big
14	05051425	b7	Prf up wind	300 +/- 50	2.5 +/- 2.5		medium	20.9	9.5	7.8	5	small
15	05051442	b7	solid up wind	300 +/- 50	2.5 +/- 2.5		medium	134.0	65	51	18.9	big
16	05050910	a4	none	300 +/- 50	2 +/- 1		small	3.5	0.1	0.3	0.2	small
17	05050935	a4	none	300 +/- 50	2 +/- 1		big	182.8	157.5	86.4	104.1	big
18	05050940	a4	prf dwn wind	300 +/- 50	1 +/- 1		medium	14.1	33.5	16.8	8.5	medium
19	05050950	a4	solid dwn wind	300 +/- 50	1 +/- 1		big	262.2	233.5	78.8	55.1	big
20	05051000	a4	prf up win	300 +/- 50	1 +/- 1		big	262.0	290	42.2	42.1	big
21	05051015	a4	solid up win	300 +/- 50	1 +/- 1		small but detectable	9.0	6.5	3	0.7	small
22	05051503	b6	none	275 +/- 15	2 +/- 1	steady wind with near-ideal data	big - not huge	171.5	52.5	66.5	22.5	big
23	05051515	b6	none	300 +/- 50	2.5 +/- 2.5		tiny - barely detectable	0.0	0.1	0.1	0.1	small
24	05051535	b6	prf dwn wind	300 +/- 50	2.5 +/- 2.5		medium-big	149.4	127	67.9	41.9	big
25	05051545	b6	solid dwn wind	300 +/- 50	2.5 +/- 2.5	slightly gusty; compare	medium	24.7	8	4	2.8	small
26	05051600	b6	prf up win	300 +/- 50	2.5 +/- 2.5		medium	33.4	23	27.4	12	medium
27	05051612	b6	solid up win	300 +/- 50	2.5 +/- 2.5		medium	21.9	49.5	10.1	9	medium
27a	05051617	b6	prf up win	300 +/- 50	2.5 +/- 2.5	same flow rate as 27			20.4	10.2	6.1	medium
27b	05051623	b6	none	300 +/- 50	2.5 +/- 2.5	same flow rate as 27; data show gas tubing			12.9	11.7	6.4	medium
28	05051035	b10	none	300 +/- 50	1.5 +/- 1.5	over manhole	small	7.7	0.1	0.2	0.1	small
29	05051045	b10	none	300 +/- 50	1.5 +/- 1.5	steady wind near end of run	big	231.9	51.5	45.3	27.2	big
30	05051100	b10	prf dwn win	300 +/- 50	1.5 +/- 1.5		medium-big; smaller than 2	84.8	96	33.5	28.1	big
31	05051110	b10	solid dwn win	300 +/- 50	1.5 +/- 1.5		medium	51.9	36	8.8	9	small
32	05051120	b10	prf up win	300 +/- 50	1.5 +/- 1.5		medium	26.8	38.5	8.3	8.4	small
33	05051130	b10	solid up win	300 +/- 50	1.5 +/- 1.5		small	2.3	5	2.3	1.2	small

Table 1. Campaign #1 Data Summary (Continued)

Segment #	Time	location	blockage	Wind Direction	Wind Speed	Comment	manual observation	DPIR+RMLD Est cfh	Spinner Avg. Est cfh	Spinner Calculated cfh (avg)	Spnner Calculated cfh (std dev)	Spinner Calc Class
34 Site A	05051705	b8	none	300 +/- 50	1.5 +/- 1.5	first upwind tray	very small	7.9	9.7	0.5	0.4	small
34 Site D	05051715		none	300 +/- 50	1.5 +/- 1.5	between b6 and b8			7			
34 Site B	05051720	b6	none	300 +/- 50	1.5 +/- 1.5	middle tray	small	0.2	0.3	0.4	0.4	small
34 Site E	05051725		none	300 +/- 50	1.5 +/- 1.5	between b4 and b6			0	-0.1	0.4	
34 Site C	05051730	b4	none	300 +/- 50	1.5 +/- 1.5	downwind tray	small	11.3	4	1.7	0.7	small
34 Site F	05051734		none	300 +/- 50	1.5 +/- 1.5	downwind of C						
34 Site G	05051738		none	300 +/- 50	1.5 +/- 1.5	downwind of F						
34 Site H	05051740		none	300 +/- 50	1.5 +/- 1.5	downwind of G			0.1	0.3	0.7	
34 A+B+C										2.6		small
35 Site A	05060823	b8	none	120 +/- 180	0.7 +/- 0.7	light rain		19.8				
35 Site D	05060830		none	120 +/- 180	0.7 +/- 0.7	light rain						
35 Site B	05060839	b6	none	120 +/- 180	0.7 +/- 0.7	light rain		27.6				
35 Site E	05060845		none	120 +/- 180	0.7 +/- 0.7	light rain						
35 Site C	05060853	b4	none	120 +/- 180	0.7 +/- 0.7	light rain		101.9				
35 Site F	05060859		none	120 +/- 180	0.7 +/- 0.7	light rain						
36 Site A	05060915	b8	per up win (east of B4)	130 +/- 30	2.5 +/- 2.5		small-medium	18.0	9.7	1.4	2	small
36 Site D	05060935		per up win (east of B4)	130 +/- 30	2.5 +/- 2.5	steady wind, sees gas from upwind			7	0.5	1.4	
36 Site B	05060940	b6	per up win (east of B4)	130 +/- 30	2.5 +/- 2.5			7.0	13	1	2	small
36 Site E	05060945		per up win (east of B4)	130 +/- 30	2.5 +/- 2.5	Good site to measure zero net flux	medium		17	0.3	3.5	
36 Site C	05060957	b4	per up win (east of B4)	130 +/- 30	2.5 +/- 2.5			21.5	missing	missing	missing	
36 A+B+C										NA		NA
37 Site A	05061015	b8	solid up win	130 +/- 30	2.0 +/- 1.5	Increasing east wind		42.9	20.6	3.9	6.3	small
37 Site D	05061022		solid up win	130 +/- 30	2.0 +/- 1.5				21.3	1.5	4.9	
37 Site B	05061030	b6	solid up win	130 +/- 30	2.0 +/- 1.5		medium	45.6	15.3	0.75	4	small
37 Site E	05061037		solid up win	130 +/- 30	2.0 +/- 1.5		medium-large flow		24.3	1.4	3.8	
37 Site C	05061043	b4	solid up win	130 +/- 30	2.0 +/- 1.5			49.2	123.3	39.6	17.2	big
37 A+B+C										44.25		big
38 Site A	05061100	b8	perf dwn win	130 +/- 30	3 +/- 1.5			43.6	17.7	7	6.1	small
38 Site D	05061103		perf dwn win	130 +/- 30	3 +/- 1.5				23.2	-3.5	4	
38 Site B	05061106	b6	perf dwn win	130 +/- 30	3 +/- 1.5			35.4	23.7	19.4	16.3	medium
38 Site E	05061111		perf dwn win	130 +/- 30	3 +/- 1.5				wrong file			
38 Site C	05061116	b4	perf dwn win	130 +/- 30	3 +/- 1.5			15.3	16.6	24.1	13.5	medium
38 A+B+C										50.5		big
39 Site A	05061132	b8	solid dwn win	130 +/- 30	3 +/- 1.5			1.7	4.8			
39 Site D	05061136		solid dwn win	130 +/- 30	3 +/- 1.5				4.1			
39 Site B	05061140	b6	solid dwn win	130 +/- 30	3 +/- 1.5			-0.7	2.5			
39 Site E	05061148		solid dwn win	130 +/- 30	3 +/- 1.5				2.8			
39 Site C	05061152	b4	solid dwn win	130 +/- 30	3 +/- 1.5			2.4	1.9			

Three methods were utilized for analyzing the data to determine approximate leak flux rates:

- 1) Comparison of DPIR and handheld RMLD concentration measurements with the calibration measurements.
- 2) Comparison of the average ppm-m value measured by the spinning RMLD (e.g. the average value of the data plotted) with calibration measurements
- 3) Calculation from first principles using Eq. (1) with data from the spinning RMLD and wind measurements. The calculations assume that the scanning RMLD laser beam traced a circle around the leak source and a steady wind from a fixed direction during the measurement period. These assumptions are simplifications, as the laser beam actually traced an ellipse and wind was generally light and variable in both speed and direction. We found that adjusting the computed flux by a factor of 1.8 resulted in very good agreement with calibration test values. This factor was applied to each of the blind data calculations. The change of wind direction relative to the orientation of the laser ellipse introduces additional error which has not yet been quantified.

Methods 1) and 2) are, in essence, measurements of methane concentration, not flux, and are expected to be reasonable approximations of flux only when the wind is similar to the wind at calibration.

Furthermore, it is expected, and the results demonstrate, that Methods 1) and 2) are not suited to estimating flux when a plume of methane originating from a source other than the immediate leak site is transported through the leak site. In that situation, the measured methane concentration (ppm or ppm-m) combines the contributions from both the upwind source carried by the plume and the local leak source, and thereby overestimates the local leak rate. *In contrast, Method 3), under steady wind conditions, deduces only the flux originating within the encircled area.*

In Table 1 we classified leak rates as “big” > 30 cfh, “medium” 10 – 30 cfh, or “small” <10 cfh. Leak rates deduced by each of the three methods (as discussed in section 8, subsection on Computing Flux for Conical-Scan Spinning RMLD) are tabulated for comparison with each other. The spinning RMLD (Method 3) results are highlighted.

Table 2 compares with the actual flow rates. Notably, the average error (=flow rate computed by Method 3/Metered flow rate) is less than 50% despite actual flow rates varying by more than two orders-of-magnitude.

Also notable are the values attained in Test Segment 35, validating the value of the spinning RMLD technique for quantifying leak flux from a local source in the presence of a plume from a separate upwind source. In this test segment, three separate leak boxes were configured in a row. The boxes were located at sites B4 (labelled as Segment 35 Site C), B6 (Segment 35 Site B), and B8 (Segment 35 Site A). The total flow to all three boxes was set by NYSEARCH and not known to the team. The flow rates to the individual boxes were not measured. We acquired direct DPIR and handheld RMLD (concentration) measurements above each of the three boxes, and spinning RMLD (flux) measurements around each box plus the areas between boxes (Segment 35 Sites E and D). Wind was generally blowing from Site C, carrying a plume from site C across Sites A, B, D, and E.

Table 2. Comparison of NYSEARCH Phase I Metered Flow Rates

NYSEARCH Test Log - Emission Quantification								
Date: May 4 - 6, 2015				Test Location: PSE&G, Edison, NJ				
Tech Provider: PSI Heath				Test Plan revision 9				
Segment	NYSEARCH :		Technology Provider :	Statistical Evaluation:		Conditions:		Obstacles
	Shape	Metered	Measured	Difference	Error	Type	Location	
Test	Test Locate	Test Plume	Emission rate	Meas-Meter	Meas/Meter			
		SCFH	SCFH	SCFH	Normal			
1	A-1 (Cal)	2.5	2.4	-0.1	0.96	None	n/a	
2	A-1 (Cal)	0.2	0.9	0.7	4.50	None	n/a	
3	A-1 (Cal)	50	51.3	1.3	1.03	None	n/a	
4	A-3	3	1.3	-1.7	0.43	None	n/a	
5	A-3	0.8	0.0	-0.8	-	None	n/a	
6	A-3	35	43.1	8.1	1.23	Perforated	DownWind	
7	A-3	48	71.8	23.8	1.50	Solid	DownWind	
8	A-3	10	9.9	-0.1	0.99	Perforated	UpWind	
9	A-3	5	15.3	10.3	3.06	Solid	UpWind	
10	B-7	0.5	0.5	0.0	1.00	None	n/a	
11	B-7	12	10.7	-1.3	0.89	None	n/a	
12	B-7	4	8.7	4.7	2.18	Perforated	DownWind	
13	B-7	35	65.7	30.7	1.88	Solid	DownWind	
14	B-7	5	7.8	2.8	1.56	Perforated	UpWind	
15	B-7	22	51.0	29.0	2.32	Solid	UpWind	
16	A-4	0.4	0.3	-0.1	0.75	None	n/a	
17	A-4	48	86.4	38.4	1.80	None	n/a	
18	A-4	12	16.8	4.8	1.40	Perforated	DownWind	
19	A-4	38	78.8	40.8	2.07	Solid	DownWind	
20	A-4	38	42.2	4.2	1.11	Perforated	UpWind	
21	A-4	1	3.0	2.0	3.00	Solid	UpWind	
22	B-6	37	66.5	29.5	1.80	None	n/a	
23	B-6	0.2	0.1	-0.1	0.50	None	n/a	
24	B-6	32	67.9	35.9	2.12	Perforated	DownWind	
25	B-6	4	4.0	0.0	1.00	Solid	DownWind	
26	B-6	11	27.4	16.4	2.49	Perforated	UpWind	
27	B-6	6	10.1	4.1	1.68	Solid	UpWind	
28	B-10	0.8	0.2	-0.6	0.25	None	n/a	
29	B-10	43	45.3	2.3	1.05	None	n/a	
30	B-10	32	33.5	1.5	1.05	Perforated	DownWind	
31	B-10	9	8.8	-0.2	0.98	Solid	DownWind	
32	B-10	9	8.3	-0.7	0.92	Perforated	UpWind	
33	B-10	1	2.3	1.3	2.30	Solid	UpWind	
34	B-4/5/6	3	2.6	-0.4	0.87	None	n/a	
35	B-4/5/6	21	n/a			None	n/a	
36	B-4/5/6	0.2	n/a			Perforated	DownWind	
37	B-4/5/6	29	44.25	15.3	1.53	Solid	DownWind	
38	B-4/5/6	29	50.5	21.5	1.74	Perforated	UpWind	
39	B-4/5/6	4	n/a			Solid	UpWind	

At Sites A, B, and C Method 1 (DP-IR/RMLD) consistently deduces an estimated flux of 40 -50 cfh (based on comparison with calibration), and Method 2 (the average value measured by the spinning RMLD compared with calibration) shows high values even at Sites D and E (between the sources) where the net flux is zero. However, the spinner flux measurements deduced by Method 3 show that the flux from all locations except Site C is small; virtually all methane is flowing from Site C and carried upwind to the other sites. *This ability to measure low (or zero) flux despite locally high concentrations from upwind sources is a vital attribute of the spinner technique. Validating its capability, albeit with some inaccuracy, is a key outcome of these tests.*

Campaign #2: Stationary Cylindrical-Scan Spinning RMLD

Campaign #1 results taught us that the conical shape of the laser light “curtain” enfolded the methane emission source complicated the analysis technique: accurate results required good knowledge of methane plume height and shape, as well as wind speed as a function of height. The Campaign #2 test configuration addressed these deficiencies by incorporating the following: a) changing the spinning scan shape to a cylinder, rather than a cone, surrounding the leak source; and b) developing software that acquires and processes the data in real-time, providing instant values of leak flux.

Data were collected at the SoCal test site in Commerce, CA following the NYSEARCH Phase II Test Plan. Table 3 summarizes the calibration and field data. 173 data files were recorded, each providing one output result, for 84 distinct locations, configuration, or flow rate, each called a test “segment”. For all segments, bottled methane flowed through a pressure regulator, needle valve, and rotameter. Thence it was transported via polyethylene tubing to each leak test location, wherein the end of the tube was buried in a box filled with sand and gravel. Typically, two or three trials were conducted for each segment, and the leak rate reported. Each test segment is defined by a number indicating its location and metered flow rate as set by the NYSEARCH test coordinator. Segments having letters a-e appended to the segment number have three individual concurrent leak sources (a, b, c) and two locations between leak sources (d, e). All but six segments were “blind” measurements wherein the flow rate was unknown to the measurement team. The remaining six measurements were made for “calibration”; these measurements differed from others only in that the actual flow rates were reported by NYSEARCH to the team.

Figure 28 plots the methane flow rate measured by spinning RMLD versus the rate indicated by the rotameter in line with the methane source tubing. There were no adjustable parameters nor data post-processing to yield these results. The measured flow rates were within +/-50% of the metered flow rates; a notable performance without adjustable parameters.

For these data, the measurement error of the averaged data is nominally 2 scfm (at flow rates < 10 scfh) or 20% of the reading (at flow rate > 10 scfh). These data were acquired with wind conditions ranging from light and variable through strong and gusty (> 5 m/s or 10 kts). It should be noted that the negative values measured with the metered flow shut off (0 scfh) are may correctly indicate that a small amount of methane is blowing, via wind gust, from outside into the laser-encircled region but not exiting during the measurement duration.

Notable are segments with suffixes d or e. These are the locations in between three concurrent leak sources. Methane emitted from the sources flows through these measurement sites, but there is no emission from within the site. As mentioned above, depending on wind, these external methane sources can and do yield negative flow rate values. These measurements indicate that, in practical use of this technology, measurement of a negative value is an indicator of a leak located outside the measurement area.

Table 3. Campaign #2 Data Summary

Segment #	Start Time	Metered Leak Rate (CFH)	Average Wind Speed (m/s)	Average Wind Direction (deg)	Measured Leak Rate (CFH)	STD DEV (+/- CFH)
Calibration 1	03071530	50			60.0	9.0
Calibration 2	03071552	10			12.2	0.7
Calibration 3	03071603	2			2.1	1.5
Calibration 4	03071618	0			-2.9	0.9
1	03071703				0.1	0.0
2	03071713				0.5	0.4
3	03071725				4.6	0.8
4	03071735				27.5	1.1
5	03071746				0.1	1.4
Calibration 5	03081105	10			9.5	0.0
6	03081110				3.7	0.2
7	03081134				11.0	1.7
7 w/barrier	03081146				-0.6	0.0
7 w/barrier + relocated Windsonics	03081156				-0.5	4.0
8	03081227				46.4	6.4
8 w/barrier	03081238				20.9	9.3
41c	03081252				2.2	0.5
41a	03081307				0.5	0.1
41b	03081319				-0.1	0.2
41d	03081330				0.2	0.4
41e	03081340				1.0	0.0
42e	03081359				3.3	0.3
42d	03081408				0.1	0.3
42c	03081418				3.1	0.2
42b	03081426				-2.3	1.2
42a	03081434				2.7	1.4
43a	03081454				10.0	2.7
43b	03081504				-5.0	1.5
43c	03081512				22.9	1.3
43d	03081521				-13.3	4.8
43e	03081530				21.9	0.3
44e	03081546				0.2	0.9
44d	03081603				-0.2	0.2
44c	03081613				-0.9	0.7
44b	03081621				-0.3	0.3
44a	03081632				-0.3	0.4
45a	03081650				-0.4	0.4
45c	03081700				-0.2	0.4
45e	03081710				0.1	0.0
46e	03081727				18.8	1.0
46d	03081735				-18.8	3.3
46c	03081747				15.9	3.2
46a	03081759				25.5	5.6

Table 3. Campaign #2 Data Summary (Continued)

Segment #	Start Time	Metered Leak Rate (CFH)	Average Wind Speed (m/s)	Average Wind Direction (deg)	Measured Leak Rate (CFH)	STD DEV (+/- CFH)
calibration 6	03091110	10			10.6	0.0
9	03091124				2.0	0.4
10	030911338				3.1	0.5
11	03091150				7.9	2.8
12	03091206				32.1	11.9
13	03091225				1.3	0.5
14	03091243				0.7	0.2
15	03091253				0.4	0.5
16	03091310				6.4	2.2
25	03091338				2.1	0.3
26	03091350				0.7	0.3
27	03091410				0.7	0.1
28	03091423				0.6	0.2
29	03091439				2.3	1.1
30	03091503				5.0	0.2
31	03091517				25.5	4.5
32	03091528				7.0	1.1
33	03091552				1.6	0.8
34	03091603				13.4	3.0
35	03091616				2.3	0.3
36	03091628				0.5	0.3
37	03091639				0.4	0.1
38	03091652				0.2	0.2
39	03091710				8.1	5.1
40	03091726				22.9	9.4
47e	03101059				0.1	0.0
47d	03101111				-0.2	0.2
47c	03101126				0.2	0.1
47b	03101139				0.0	0.1
47a	03101151				-0.2	0.1
48a	03101212				-0.1	0.1
48c	03101222				0.2	0.1
48e	03101232				0.2	0.0
49e	03101246				0.3	0.1
49c	03101258				1.6	0.1
49a	03101308				1.4	0.0
50a	03101326				4.2	2.4
50b	03101335				-0.1	1.5
50c	03101350				8.9	2.3
50d	03101358				-2.5	0.0
50e	03101406				2.3	0.6

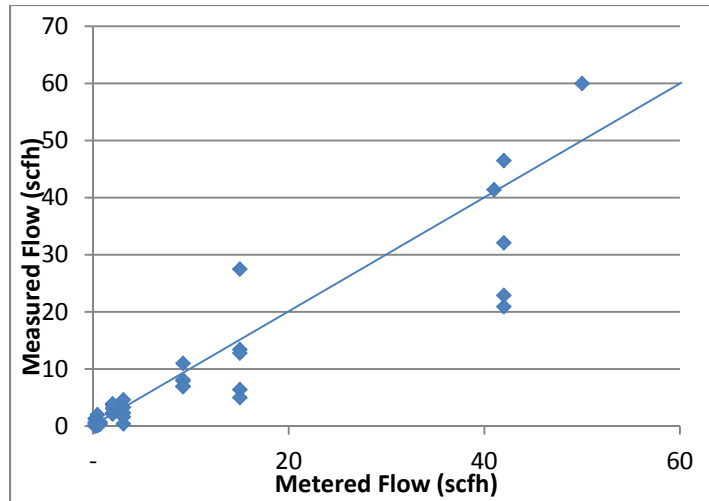


Figure 28. Methane Flux measured by spinning RMLD vs flow rate measured by rotameter in line with the gas supply during campaign #2 tests.

Campaign #3: Conical-Scan Spinning RMLD with Adjustable Aim

In the third campaign of tests, the vehicle roof-mounted conical configuration was re-adopted with the intent of evaluating its ability to measure flux of real-world (rather than manufactured) gas leaks without equipment or operators having to exit vehicle. This capability was requested by the test providers. Furthermore, to accommodate measuring leaks located at various distances from the vehicle, sometimes in partially blocked or optically obscured areas (e.g. behind hedges), the angle of the “spinner”, and thus the cone axis relative to the ground, was made to be adjustable.

Table 4 summarizes the data collected at 15 locations in Westchester County, NY, near the ConEd facility in Elmsford and in accordance with NYSEARCH Phase III Test Plan. Each “Measured Emission Rate” is deduced from at least 10 rotations of the laser scan around the leak source.

It is noted that the day prior to onset of testing was marked by heavy rain and flooding in the test area. The saturated ground suppressed much of the leakage that the tests were intended to measure. Therefore, many of the sites recorded very small (or sometimes negative) flow rates. This is not a result of the conical measurement geometry.

Table 4 documents additional information derived from the raw data. It presents the flux measured for each laser scan rotation, computes the “Measured Mean Flux” for each set of ten or more rotations (reported as Measured Emission Rate in Table 4), and the Standard Deviation (“Stdev”) of the individual flux measurements. Qualitatively, the ratio (Stdev)/(Mean Flux) is an measure of reproducibility and thus confidence in flux accuracy.

Table 4 also documents path-integrated methane concentration near the leak site in terms of ppm-m as measured directly by RMLD. Using all data points (typically 2500 – 5000) embodied in each data file of ten or twenty rotations, the “Average” and “Peak” ppm-m values are reported. Generally, average values were less than 20 ppm-m, typical of 2 – 3 ppm ambient background methane over a 5 – 10 m path length, while peak values varied from a few tens of ppm-m to several hundred ppm-m depending on leak rate and wind conditions. In some cases, “Average ppm-m” exceeded 100, indicating relatively high concentration of gas throughout the measurement site, not necessarily in a well-defined plume or with high flux. This could occur with stagnant wind or a gas source originating outside the area of interrogation.

A review of the data indicates that wind variability was the most significant contributor to low-confidence data (i.e. high Stdev). Most measurements occurred in conditions of “light and variable” wind, wherein the wind measured at the roof of the vehicle differed from the wind at the leak site, albeit only a few meters distant. This led to errors in the flux calculations; these errors diminished with averaging over several rotations. Three significant examples (Leak ID#3, #4 and #8 listed in Table 4) are further discussed here.

Leak ID#4: This set of ten rotations is a nearly optimum measurement as shown in Figure 29. It experienced relatively steady wind and exhibited a well-defined plume aligned with the wind. Stdev/(mean flux) is low (0.4).

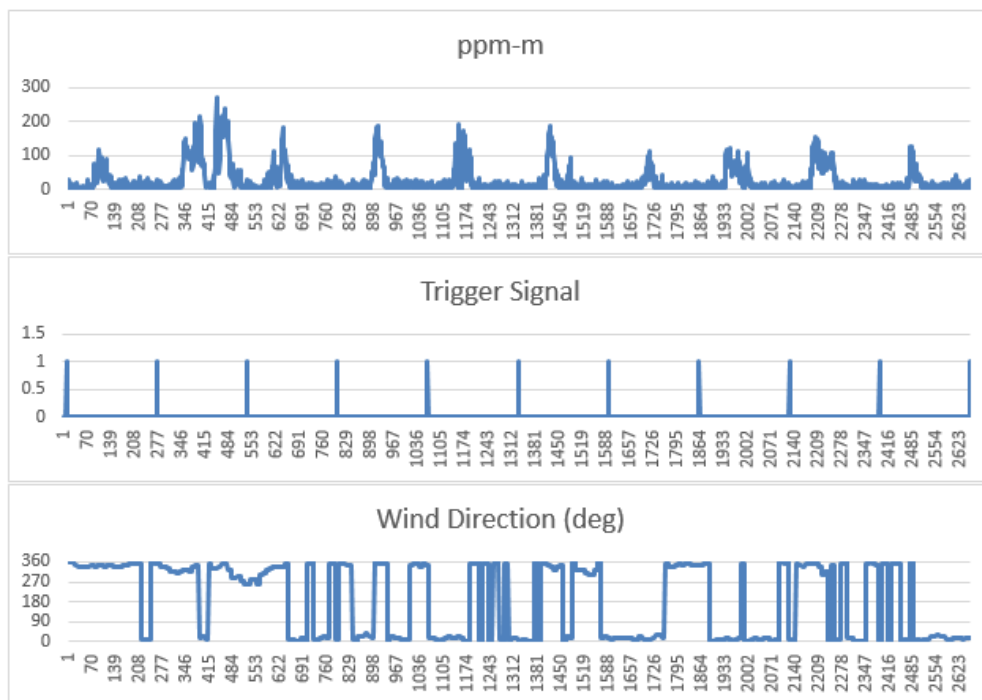


Figure 29. Leak ID#4. Top: Path-Integrated Concentration vs time (each point = 0.1 s). Middle: Trigger signal indicating spinning laser is pointing North. Bottom: Wind direction measured at vehicle roof. Ppm-m displays spikes as the laser beam crosses the gas plume upon each rotation. The spikes nominally lag the trigger by 180 deg, indicating the laser is pointing South when it crosses the plume. Therefore, the plume is blowing from the North, correlating well with the measured wind direction.

Leak ID#3: The emission from a sewer drain is characterized by high average ppm-m but low mean flux with high standard deviation. Figure 30 shows a photograph of the vehicle next to a sewage drain.

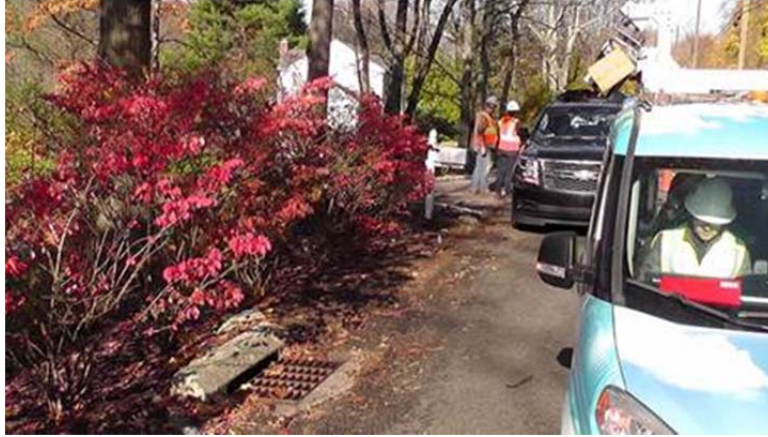


Figure 30. Scanning of sewer drain using the Conical-Scan Spinning RMLD.

The individual flux calculations for each laser rotation exhibited large values, both positive and negative, which *average to near zero*. The ppm-m data illustrated periods of high concentration lacking a well-defined plume during periods of generally easterly wind yet saw essentially no gas during periods of generally southerly winds (Figure 31). This indicates a relatively large methane source and sink, but not a continuous leak. The sewer drain was a likely source and sink of sewer or swamp gas, though another gas source located outside and to the east of the interrogated region was possible.

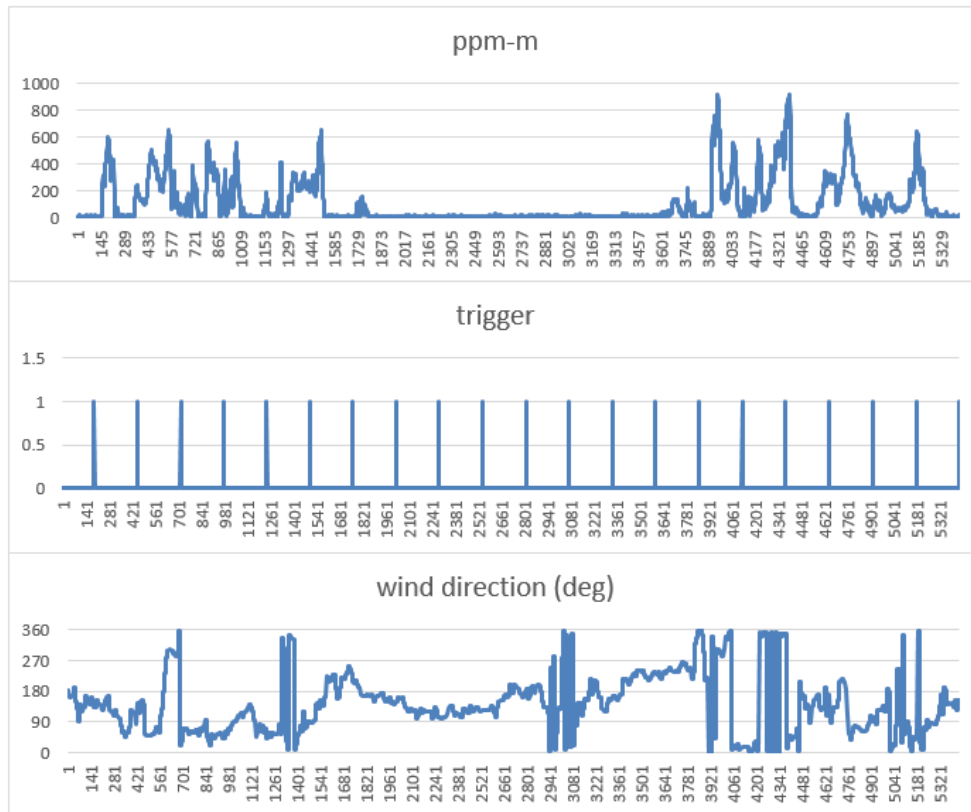


Figure 31. Time series plots with data from sewer drain.

Leak #8 and 9: These leaks were at the same location representing a complex blockage scenario. The FLUX Mobile was parked near the street curb while the leak was located on a lawn behind a row of hedges. The laser cone swept over the hedges to circumscribe the leak. Real-time calculations consistently yielded negative values of mean flux, initially attributed to the inaccuracy of the conical geometry. However, post-analysis of the data revealed a well-defined plume generally blowing nearly perpendicular to the measured wind. The difference in wind direction is attributed to the influence of the hedges on the local wind. Upon post-processing to artificially rotate the wind direction by 240 deg for Leak ID#8 (Figure 32) and 270 deg for Leak ID#9, the computed mean flux values changed to 13.4 and 10.1 scfh respectively, as reported in Table 4.

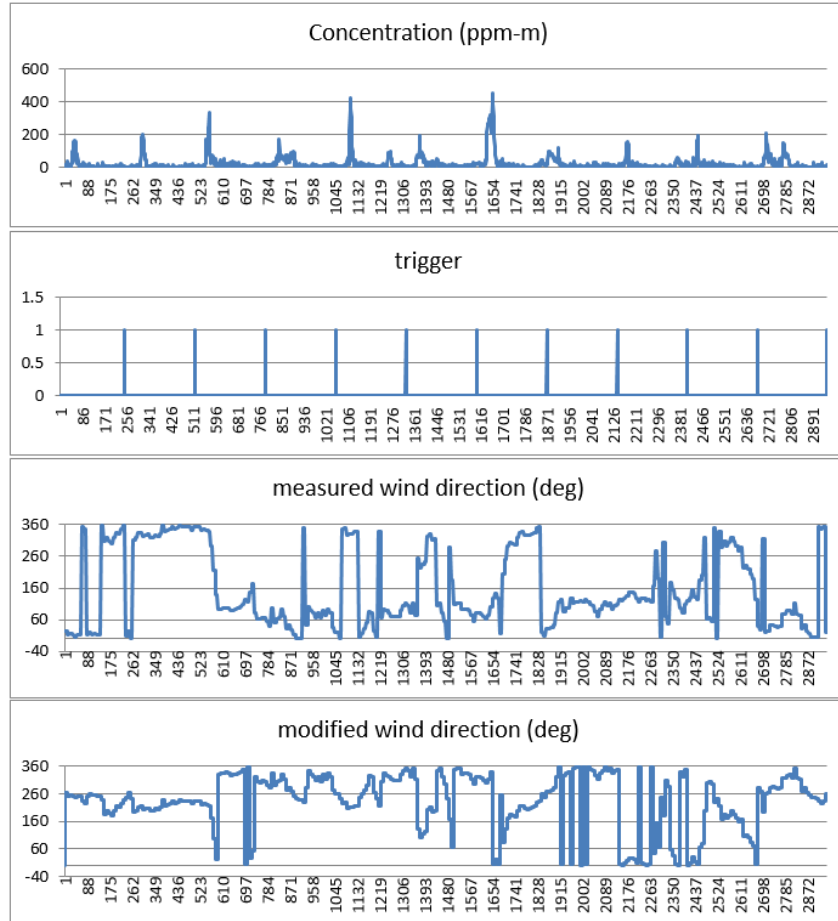


Figure 32. Leak ID#8. Top: ppm-m data showing spikes indicative of leak plume. Plume spikes lag trigger by approximately 60 deg, indicating plume blows from Southwest. Wind measured at vehicle is predominantly North or East, resulting in poor calculation of flux. Mathematically modifying the wind direction to be predominantly Southwest and North (240 deg rotation) improves the calculation.

Campaign #4: Field Tests with Advanced Mobile Units in Las Vegas

From March to December of 2016, over 400 leak surveys were conducted. The monthly distribution of surveys is shown below, Figure 33, with a monthly average of 30 surveys. The survey vehicles were equipped with several sensors, as illustrated in Figure 23. The lead car was instrumented with one optical methane detector in the front and with two technicians holding a RMLD each. The following advanced mobile car had two fixed RMLDs and mounted on top of the car. The Herriott cell extractive analyzer

(HC) is installed in the back of the vehicle and sample gas is drawn from the front-center of the vehicle. Distance between the two cars is maintained between 2-10 vehicle-length apart.

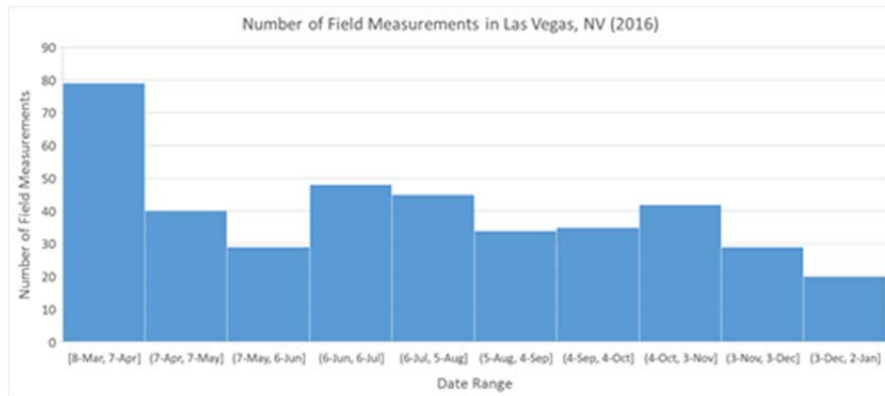


Figure 33. Distribution of field measurements conducted in Las Vegas, NV (2016).

Figure 34 shows a sample time series of methane concentration (ppm-m) from two side scanning RMLDs. As indicated on the figure, the driver side’s RMLD picked up a leak and not the passenger side. Most leaks will be identified on the passenger side, the side closest to the roadsides where the gas distribution lines are located. Leaks seen on the driver side are probably due to the wind transporting the plume from the other side of the road toward the car or a large plume traversing the road from right to left. In some instances, there might be an actual leak emanating from the center of the road. A leak detected by both RMLDs may indicate a large plume or a plume that traverses the road from passenger to the driver side (due to wind direction).

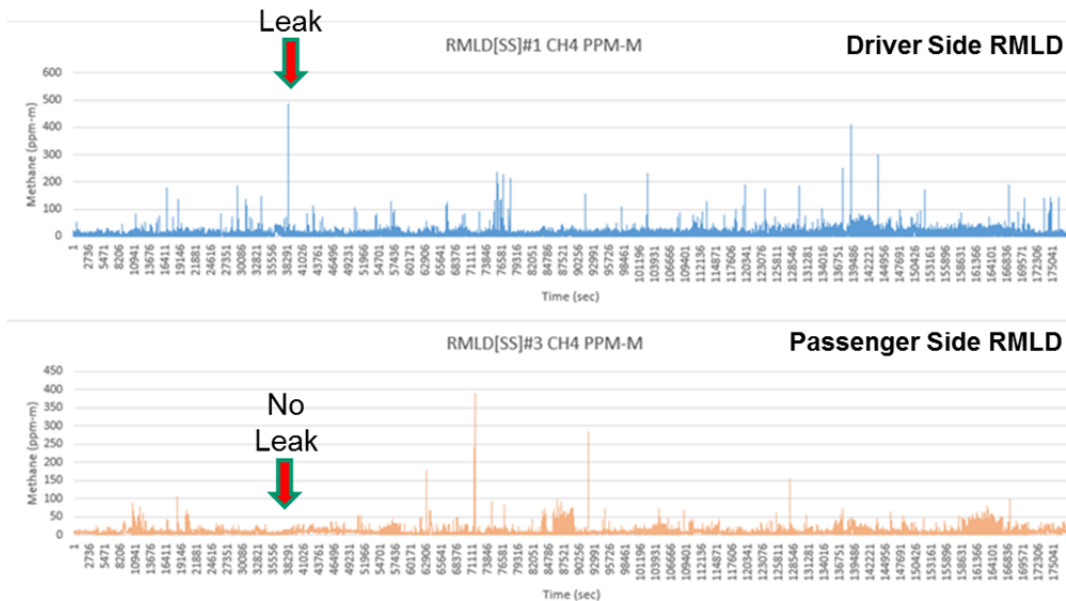


Figure 34. Sample data from fixed RMLDs during a survey trip.

Figure 35 plots all the alarms recorded by both RMLDs during each survey trip. This plot clearly indicates that most of the recorded alarms originated from the Passenger Side RMLD as one would have expected. There appears to be at least four times more recorded leaks from the Passenger Side RMLD

than the Driver Side RMLD. However, the leaks picked up by the Driver Side RMLD are certainly not negligible by any means.

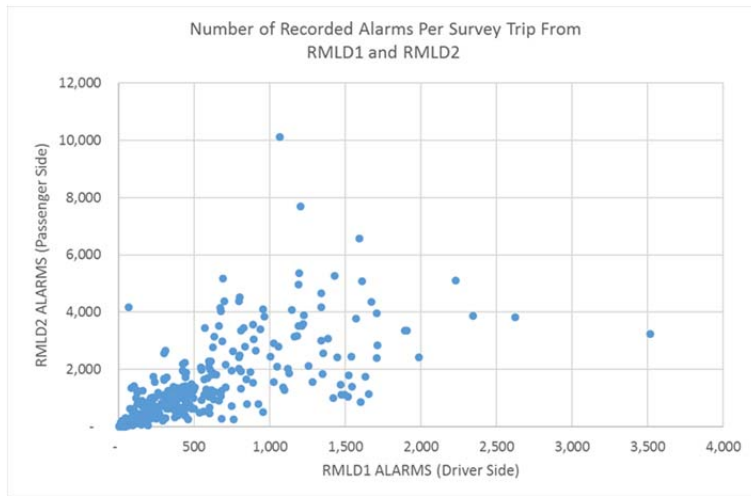


Figure 35. Comparing number of alarms from RMLDs installed in Passenger and Driver sides.

Figure 36 compares the percent of alarms from RMLD1, RMLD2 and combination of the two (i.e. when both RMLDs alarmed). An overwhelming 70% of the alarms originated from RMLD2 alone (Passenger Side), and near 30% from the Driver Side RMLD. Both RMLD1 and RMLD2 alarmed at the same time for only a tiny fraction of a percent in all recorded instances. The data indicate that having two RMLDs (one at each side of the car) is beneficial for catching different leak sources and expanding the surveyed areas.

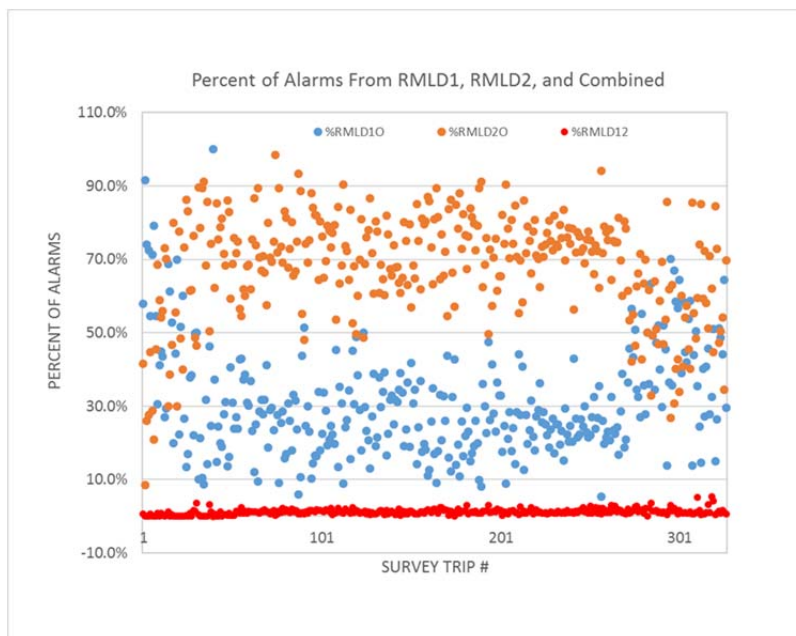


Figure 36. Distribution of leaks detected by two fixed RMLDs.

Figure 37 plots the percent of alarms that are simultaneously triggered by both RMLDs (red dots). The result further indicates that the two RMLDs alarm simultaneously very infrequently; thus a two-system RMLD would be beneficial for any leak survey deployment.

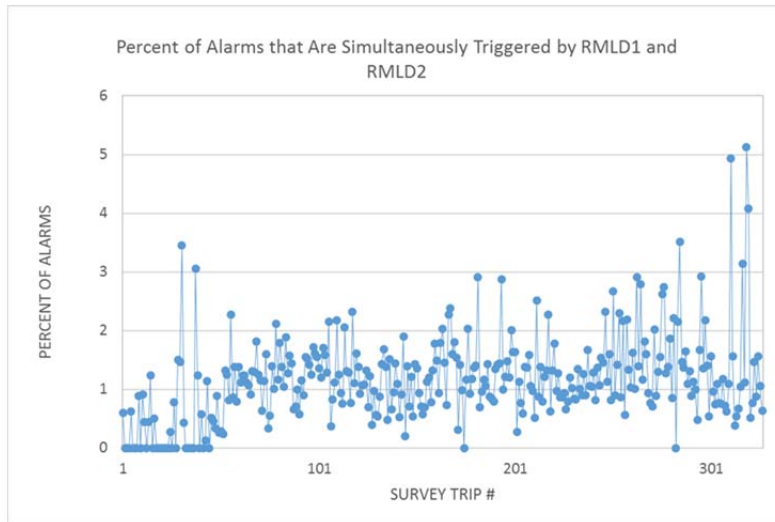


Figure 37. Frequency of leaks detected by both fixed RMLDs simultaneously.

The extractive gas analyzer sampled ambient gases from the front-center of the vehicle. Figure 38 shows the percent of alarms from the analyzer compared to the total alarms from the RMLD1 and RMLD2. In most of the surveys, the analyzer contributed a tiny fraction of the total alarms. The time response of the analyzer due to the sampling tube length and the vehicle’s speed have the potential to minimize the efficacy of the analyzer in detecting gas leaks in typical urban surveys. Moreover, the higher sensitivity analyzer may be needed to detect very low gas concentrations.

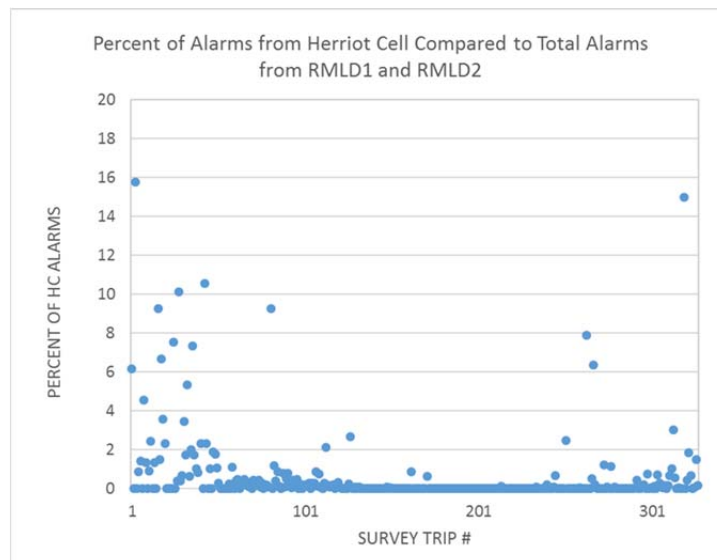


Figure 38. Efficacy of extractive method in detection of leaks when compared to fixed RMLDs.

Key lessons and observations from the data analyzed are summarized:

- At vehicle speed of 5 mph, plumes having dimensions less than 1 ft are detected by the RMLD with its 10 Hz data rate (0.1 s response time). In contrast, the 1s response time of the extractive Herriot cell sensor confounds detecting plumes narrower than a few feet.
- The extractive sensor is designed with a detection limit (signal-to-noise ratio =1) of 0.5 ppm at 1 Hz bandwidth. The instrument alarm threshold is set at 10x the detection limit, 5 ppm. Therefore, it will alarm upon detecting a plume having an average concentration 5 ppm averaged over 7.3 ft when surveying at 5 mph, or averaged over 22 ft when surveying at the more typical 15 mph. Stated differently, for a 1 ft plume dimension, the concentration that activates an alarm is 110 ppm. The actual plume dimension and concentration depends on the flow rate and wind, especially wind direction relative to vehicle direction.
- We have observed some drift in the baseline methane measurement with the extractive sensor. The baseline is nominally 2 ppm (typically ambient methane), and we observe slow variations of comparable magnitude. This drift occurs over times scales of minutes and thus cannot be attributed to local leak sources. Therefore, it is either an instrumental drift of the zero point (or offset), or real changes in background ambient methane.
- Using two RMLDs increases the area of survey and the likelihood of detecting leaks.

Campaign #5: Field Tests with RMLD-QGI Field Prototype in California:

With test sites provided by SoCalGas (Pico Rivera, CA) the field prototype RMDL-QGI was subjected to real-world leak scenarios over a period of 4 days in accordance with NYSEARCH Phase IV Test Plan. Calibrated leak sources and urban leak locations were measured daily. Figure 39 shows a controlled leak used for calibrating the measurement system. Figure 40 shows an uncontrolled leak from a hole in the lid of a water box during a survey trip. The evolution of the leak can be discerned from the frames. These images provided three key pieces of information including dynamics of the leak plume, location of the leak, and leak rate.

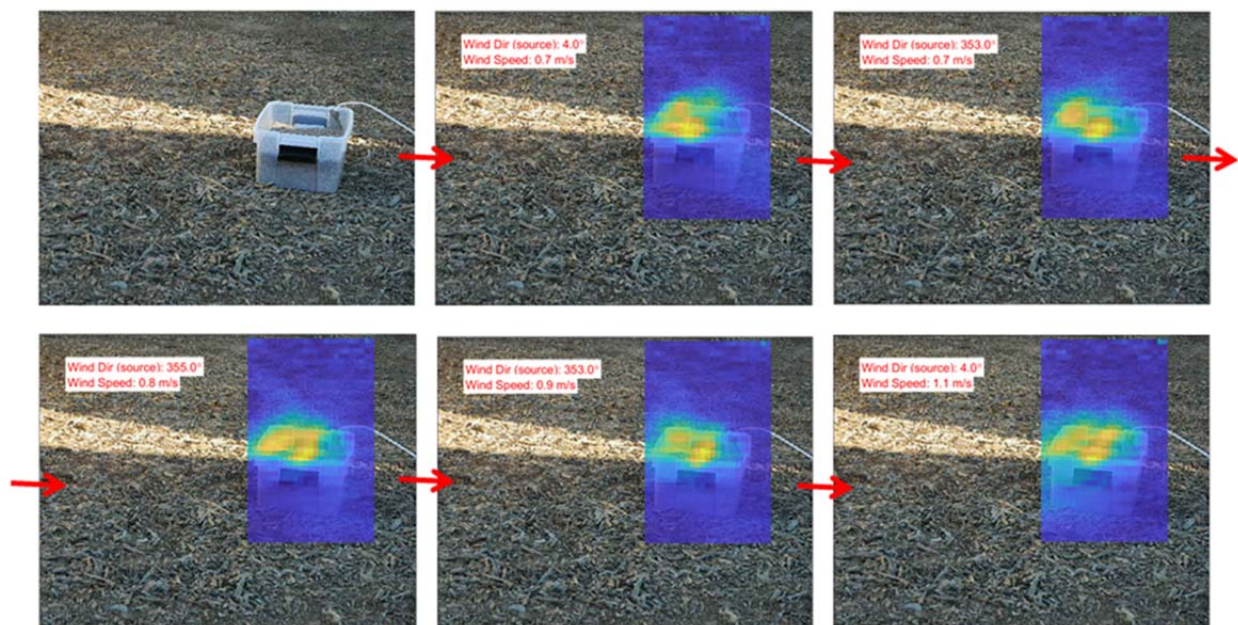


Figure 39. A sequence of frames (1 Hz) collected during a 5 SCFH controlled leak scenario at the Pico Rivera, CA SoCal facility.

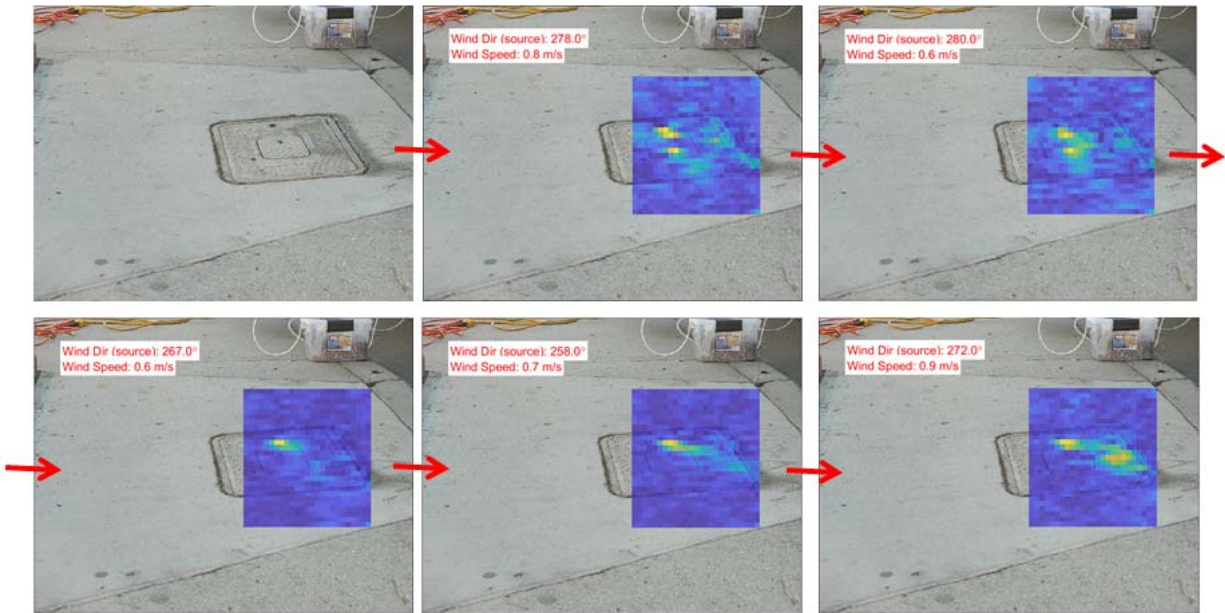


Figure 40. An uncontrolled, fugitive emission stemming from a hole in the lid of a water box. Sequence of images at 1 Hz.

The instrument was calibrated using five separate controlled leak scenarios, two of which were conducted at the PSI facility in Andover, MA, and the other three being conducted at the SoCal facility. A summary of the calibration statistics in terms of accuracy and precision is listed in Table 5, below.

Table 5. Accuracy and Precision Statistics for Controlled Leak Scenarios Using the RMLD-QGI

Metered Leak Rate [scfh]	Measured Leak Rate [scfh]	Error [scfh]	% Error	Standard Deviation [scfh]	# of Frames	Location
27.5	26.6	0.9	3.3%	16.8	16	PSI
13.8	14.7	0.9	6.5%	6.1	16	PSI
5	7	2	40.0%	1.6	23	SoCal
1	1.2	0.2	20.0%	0.5	12	SoCal
0.5	4.7	4.2	840.0%	1.1	19	SoCal

It should be noted that for the start of day validation tests conducted on December 12, 2017, the instrument was encountering power issues (originating from the supplying power inverter). This issue was resolved for all further tests. Additionally, mechanical issues on the mounting of the anemometer required that the anemometer rest atop the base vehicle, held in position by hand for all tests.

A total of 51 tests were conducted and analyzed (three of which were known controlled leaks, found in the table above). Precision statistics for these tests can be found in Table 6. Accuracy statistics will be computed upon receipt of validation measurements.

Table 6. Campaign #5 Data Summary

Test #	Location ID	Date	Time	Address # (Date Dependent)	Site #	# of Frames	Avg. Wind Speed [m/s]	Avg. Wind Dir [deg] (relative to sensor dir)	Avg. Flux [scfh]	Std. Flux	Notes
1	1	171212	8:54	Situation City	Validation Test 1	9	1.3	19	10.7	7.2	Potentially malfunctioning sensor, power inverter issues
2	1	171212	9:30	Situation City	Validation Test 2	12	1.7	178	74.4	20.3	Potentially malfunctioning sensor, power inverter issues
3	1	171212	9:58	Situation City	Validation Test 3	11	1.1	140	32.1	15.9	Potentially malfunctioning sensor, power inverter issues
4	2	171212	11:52	Address 1	Point 2	15	0.5	159	2.4	0.7	
5	2	171212	12:02	Address 1	Point 2, Tracer	10	1.1	146	13.7	5.7	
6	2	171212	12:15	Address 1	Point 3	18	0.6	65	1.6	0.4	
7	2	171212	12:26	Address 1	Point 3, 4, 5	14	0.2	143	0.8	0.4	
8	2	171212	12:41	Address 1	Point 6	12	0.5	154	7.3	2.5	
9	2	171212	12:52	Address 1	Point 1	14	0.9	310	4.2	0.7	
10	3	171212	13:51	Address 2	Point 1, 2	18	0.9	218	1.4	0.5	
11	3	171212	14:00	Address 2	Point 1, 2, Tracer	14	1.8	272	3.6	0.6	
12	3	171212	14:11	Address 2	Point 3	14	1.5	286	4.8	1.4	
13	4	171212	15:14	Address 3	Point 1	18	1.5	289	5.3	1.5	Repeats of point 1 for alignment
14	4	171212	15:21	Address 3	Point 1, Tracer	16	0.8	316	6	1.7	Bucket not shown in gif
15	6	171212	16:07	Situation City	Validation Test 1	16	0.8	256	5	3	
16	6	171212	16:26	Situation City	Validation Test 2	20	0.4	267	5.4	1.6	
17	7	171213	8:32	Situation City	Validation Test 1	23	0.9	143	7	1.6	
18	7	171213	8:51	Situation City	Validation Test 2	12	0.5	136	1.2	0.5	
19	7	171213	8:59	Situation City	Validation Test 3	19	0.9	90	4.7	1.1	
20	9	171213	10:28	Address 2	Point 1	18	0.8	275	9.9	2.8	
21	9	171213	10:37	Address 2	Point 1, Tracer	13	0.5	263	5.7	2.5	Bucket covering leak...
22	9	171213	11:00	Address 2	Point 2	16	0.4	94	5.3	1.5	
23	9	171213	11:12	Address 2	Point 3	21	0.4	253	1.7	0.6	
24	10	171213	13:32	Address 3	Bar Hole 1, 2	28	0.8	165	2.4	1.1	
25	10	171213	13:45	Address 3	Bar Hole 4	16	1.6	154	3.9	1.2	
26	10	171213	13:56	Address 3	Bar Hole 3, 5	12	1	169	4.6	2.4	
27	10	171213	14:03	Address 3	Bar Hole 3, 5, Tracer	21	1.3	159	9.9	2.6	
28	10	171213	14:11	Address 3	Bar Hole 6	13	3	191	21	3.3	
29	10	171213	14:30	Address 3	Bar Hole 7, 8	22	0.9	90	4.5	1.9	
30	10	171213	14:42	Address 3	Bar Hole 9, 10, 11	24	1.4	184	6	1.2	
31	10	171213	14:59	Address 3	Bar Hole 12	30	1.6	188	6.8	1.6	
32	12	171213	16:06	Situation City	Validation Test 1	14	0.6	196	8.2	5.4	
33	12	171213	16:14	Situation City	Validation Test 2	20	1.2	217	38.5	13.7	
Test #	Location ID	Date	Time	Address # (Date Dependent)	Site #	# of Frames	Avg. Wind Speed [m/s]	Avg. Wind Dir [deg] (relative to sensor dir)	Avg. Flux [scfh]	Std. Flux	Notes
34	13	171214	8:56	Situation City	Validation Test 1	12	0.9	100	13.9	3.3	
35	13	171214	8:47	Situation City	Validation Test 2	17	0.8	121	18.8	6.5	
36	14	171214	10:05	Address 1	Point 1	14	0.4	113	1.1	0.4	reflections or residual methane from DPIR in scene
37	14	171214	10:18	Address 1	Point 1, Tracer	24	1.2	129	6	1.6	
38	14	171214	10:28	Address 1	Point 2	12	0.6	258	0.6	0.6	erroneous spikes in wind speed averaged out
39	14	171214	10:41	Address 1	Point 3	10	0.9	228	2.8	1.5	
40	15	171214	11:32	Address 2	Point 1	15	1.2	339	3.4	1.1	
41	15	171214	11:28	Address 2	Point 1, Tracer	16	2.1	36	11.1	2.9	
42	15	171214	11:40	Address 2	Point 2	16	0.4	251	1.5	1	
43	16	171214	12:13	Address 3	Point 1	14	0.6	148	2.4	0.9	
44	16	171214	12:21	Address 3	Point 2	18	0.9	270	1.8	0.8	
45	16	171214	12:29	Address 3	Point 2, Tracer	19	0.8	295	4.5	1.3	
46	17	171214	13:14	Address 4	Point 1	20	1	271	2.7	0.8	
47	17	171214	13:25	Address 4	Point 1, Tracer	40	1	187	6.6	2.7	
48	17	171214	13:33	Address 4	Point 2	16	0.7	206	1.6	1.5	erroneous spikes in wind speed averaged out
49	18	171214	14:59	Situation City	Validation Test 1	17	1.1	293	7.9	2.6	
50	18	171214	15:08	Situation City	Validation Test 2	17	1	301	20.4	7	
51	18	171214	15:16	Situation City	Validation Test 3	19	0.9	247	14.2	9.6	

Based on results from known, controlled leaks analyzed, this technology has proven the capability to estimate leak rate by using the RMLD in an imaging configuration. Not only does it provide a means to deduce leak rate, but it provides the user with a simple means to localize the leak, visually. *This was the first-ever quantitative imaging of small fugitive emissions using this active laser technology which is independent of ambient environmental conditions.* The work has been presented at several technical conferences with corresponding publications (see Section 14 below). The accuracy of the flux estimations diminishes unless the wind is measured close to the leak source. Future R&D (beyond the scope of this project) is expected to: a) improve the flux algorithms by mitigating the effects of the wind variability on accuracy; and b) ruggedize and miniaturize the benchtop setup to a portable and self-contained sensor platform.

11. Task 7: Peer Review

The first Peer Review Meeting was held on May 2016 and the second one on May 2017. Presentation slides from these meetings were provided to PHMSA.

12. Task 8: Quarterly Progress Reports

A total of eight quarterly reports were submitted and completes this task.

13. Task 9: Final Report

The submission of this Final Report completes this task.

14. Conferences and Publications

Results of this work were presented at several conferences. A list of these attended conferences is provided below.

- Methane Detection Technology Open Forum
 - Colorado State University, Ft. Collins CO (Sept 26, 2016)
 - Presentation: Mickey Frish, RMLD Sentry for Upstream Natural Gas Leak Monitoring
- 2016 MIRTHER Symposium on Regional Air Quality Monitoring in Safety and Security Applications
 - City College of New York, New York, NY (August 2016)
 - Panel Presentation: Matthew Laderer, Emerging Mobile and Airborne TDLAS Methods for Environmental and Explosion Safety
- Field Laser Applications in Industry and Research (FLAIR) 2016
 - Aix-les-Bains France (September 12, 2016)
 - Booth, Poster and Presentation: Mickey Frish, TDLAS Methods for Detecting, Locating, and Quantifying Methane Emissions
 - Booth and demonstration
- ARP Ae Technology Showcase
 - Washington, DC, Feb 28 - Mar 1, 2017
 - Booth with demonstration
- SPIE Commercial and Scientific Sensing Conference
 - Anaheim, CA (April 10-12, 2017)
 - Presentation and Paper: Richard T. Wainner, Nicholas F. Aubut, Matthew C. Laderer, Michael B. Frish, “Scanning, standoff TDLAS leak imaging and quantification”
 - Panel Presentation: Mickey Frish, Emerging Mobile and Airborne TDLAS Sensors for Natural Gas Leak Quantification
- OSA Conference on Lasers and Electro-Optics (CLEO)
 - San Jose, CA (May 15, 2017)
 - Invited Presentation: Mickey Frish, Laser-Based Sensors for Addressing Climate Change
- MONITOR Year 2 Annual Meeting
 - Ft. Collins CO, May 23-24, 2016
 - Presentation, Booth Display, Poster
- U.S. Department of Energy, Mastering the Subsurface through Technology Innovation, Partnerships and Collaboration: Carbon Storage and Oil and Natural Gas Technologies Review Meeting

- Pittsburg, PA (AUGUST 1-3, 2017)
- Poster: Michael B. Frish and Shin-Juh Chen, “Laser-Based Sensors for MVA at Wellheads and Subsurface Storage Sites”
- PRCI Meeting
 - Miami, FL, Mar 5-7, 2018
 - Poster: Michael B. Frish and Shin-Juh Chen, “Remote Methane Leak Detection – Quantitative Gas Imager (RMLD-QGI), Low-Cost Laser-Based Natural Gas Imager with Leak Rate Estimation for LDAR and Pipeline Survey”
- ARP Ae Technology Showcase
 - Washington, D.C., Mar 13-15, 2018
 - One-page handout on RMLD-QGI were distributed
 - Booth with demonstration
- OSA Imaging and AO Conference
 - Orlando, FL, Jun 25-28, 2018
 - Presentation and Paper: Richard T. Wainner, Nicholas F. Aubut, Matthew C. Laderer, Shin-Juh Chen, and Michael B. Frish, “Handheld, Quantitative, Standoff Methane Detector and Imager”
- World Gas Conference
 - Washington D.C., Jun 25-29, 2018
 - Presentation: Michael B. Frish, “Scanning, Standoff Laser-Based Leak Imaging and Quantification”
- FLAIR 2018
 - Assisi, ITALY, Sep 10-14, 2018
 - Presentation: Nicholas F. Aubut, Richard T. Wainner, Shin-Juh Chen, and Michael B. Frish, “Quantitative Gas Imager and Leak Rate Estimator”

15. Summary and Conclusions

This PHMSA R&D project successfully met the overall objective to develop and assess performance of survey technologies and methodologies to locate and quantify flux of non-hazardous natural gas leaks. All the technical tasks were completed and the deliverables were furnished to PHMSA. This DOT-funded research with cost-share from Heath Consultants Inc. has generated much interest from the gas survey industries and led to additional and complementary field tests through in-kinds and funds from NYSEARCH, SoCal, PG&E, Heath and PSI.

Spinning RMLD using cylindrical and conical-scan were utilized to survey real world leak scenarios. Software and graphical user interface were developed to perform system control, data acquisition, processing, analysis, recording, GPS positioning, and reporting functions to facilitate leak surveys in urban environments. Using two surveying vehicles, extractive analyzer, fixed and handheld open-path sensors, and wind sensor were installed and operated for almost a year without incidence of any major mechanical failure from any of the sensors. A field prototype imaging leak system (a first of its kind to our knowledge) was successfully assembled and tested in real-world leak scenarios in the vicinity of the SoCal facility in Pico Rivera, CA, in 2017.

16. Acknowledgment

The authors gratefully acknowledge the valuable technical contributions of the following individuals:

Physical Sciences Inc.

Joy Stafford
Matt Laderer
Oscar Herrera
Nick Aubut
Richard Wainner
Seth Abramczyk

Heath Consultants Inc.

Jim Rutherford
Steve Chancey
Mireily Mir
David Nash
Juan Ortiz
Meredith Therrien
Jeff Parker

NYSEARCH

Joe Mallia
Daphne D’Zurko

PSE&G

George Ragula

SoCal

Ed Newton
Gilbert Ching

PGE

Gerry Bong

University of Houston

Lydia Yang